Received: 15 January 2020 | Revised: 4 May 2020 | Accepted: 13 May 2020

DOI: 10.1002/prot.25901

PROTEINS WILEY

RESEARCH ARTICLE

Zinc binding promotes greater hydrophobicity in Alzheimer's Aβ42 peptide than copper binding: Molecular dynamics and solvation thermodynamics studies

Subramanian Boopathi[1] | Pham Dinh Quoc Huy[2] | Wendy Gonzalez[1,3] | Panagiotis E. Theodorakis[2] | Mai Suan Li[2,4]

[1]Centro de Bioinformática y Simulación Molecular (CBSM), Facultad de Ingeniería, Universidad de Talca, Talca, Chile

[2]Institute of Physics, Polish Academy of Sciences, Warsaw, Poland

[3]Millennium Nucleus of Ion Channels-Associated Diseases (MiNICAD), Universidad de Talca, Talca, Chile

[4]Institute for Computational Science and Technology, Quang Trung Software City, Tan Chanh Hiep Ward, Ho Chi Minh City, Vietnam

Correspondence
Subramanian Boopathi and Wendy Gonzalez, Centro de Bioinformática y Simulación Molecular (CBSM), Facultad de Ingeniería, Universidad de Talca, Talca, Chile.
Email: boopathialzheimer@outlook.com (S. B) and
Email: wgonzalez@utalca.cl (W. G.)
Panagiotis E. Theodorakis and Mai Suan Li, Institute of Physics, Polish Academy of Sciences, Warsaw, Poland.
Email: panos@ifpan.edu.pl (P. E. T.) and
Email: masli@ifpan.edu.pl (M. S. L.)

Funding information
National Science Centre, Poland, and Department of Science and Technology, Ho Chi Minh city, Vietnam., Grant/Award Number: 2015/19/P/ST3/03541; University of Talca; the "Fondo de Atracción de postdoctorado carácter Internacional" scheme.; European Union's Horizon 2020 research and innovation programme under the Marie Skłodowska-Curie grant agreement, Grant/Award Number: 665778; PLGrid Infrastructure.; ANID-FONDECYT (Fondo Nacional de Desarrollo Cientifico y Tecnologico), Grant/Award Number: 1191133 and ANID-FONDEQUIP EQM160063; Polish NCN., Grant/Award Number: 2015/19/B/ST4/02721

Peer Review
The peer review history for this article is available at https://publons.com/publon/10.1002/prot.25901.

Abstract

The aggregation of Aβ42 peptides is considered as one of the main causes for the development of Alzheimer's disease. In this context, Zn^{2+} and Cu^{2+} play a significant role in regulating the aggregation mechanism, due to changes in the structural and the solvation free energy of Aβ42. In practice, experimental studies are not able to determine the latter properties, since the Aβ42–Zn^{2+} and Aβ42–Cu^{2+} peptide complexes are intrinsically disordered, exhibiting rapid conformational changes in the aqueous environment. Here, we investigate atomic structural variations and the solvation thermodynamics of Aβ42, Aβ42–Cu^{2+}, and Aβ42–Zn^{2+} systems in explicit solvent (water) by using quantum chemical structures as templates for a metal binding site and combining extensive all-atom molecular dynamics (MD) simulations with a thorough solvation thermodynamic analysis. Our results show that the zinc and copper coordination results in a significant decrease of the solvation free energy in the C-terminal region (Met35-Val40), which in turn leads to a higher structural disorder. In contrast, the β-sheet formation at the same C-terminal region indicates a higher solvation free energy in the case of Aβ42. The solvation free energy of Aβ42 increases upon Zn^{2+} binding, due to the higher tendency of forming the β-sheet structure at the Leu17-Ala42 residues, in contrast to the case of binding with Cu^{2+}. Finally, we find the hydrophobicity of Aβ42–Zn^{2+} in water is greater than in the case of Aβ42–Cu^{2+}.

KEYWORDS
Alzheimer's disease, and hydrophobicity, Aβ42, copper, molecular dynamics, solvation thermodynamics, zinc, β sheets

1 | INTRODUCTION

In 1901, a 50-year-old patient, who was later diagnosed with Alzheimer's disease (AD), was hospitalized because she had untreatable paranoid symptoms, such as sleep disorders, disturbances of memory, aggressiveness, crying, and progressive confusion. Symptomology worsened more and more until her death in 1906. In this regard, the report of doctor Alois Alzheimer's noted distinctive plaques and neurofibrillary tangles in the brain histology. However, it was only in 1998 that plaques were pointed as one of the main reasons for the development of AD.[1] AD is a common age-related neurodegenerative disorder, affecting an estimated 48.6 million patients worldwide over the age of 60. It is projected that over the next 40 years this figure will reach more than 130 million people.[2] In general, AD is characterized by extracellular abnormal deposition of Amyloid-β (Aβ) peptides inside the brain tissues. These deposits are known as amyloid plaques. In the case of a healthy brain, the Aβ is soluble and exists in monomeric forms. However, in the case of a brain affected by AD, Aβ peptides tend to aggregate into oligomers and then into fibrils, which assemble into senile plaques.[3,4] While Aβ is produced by cleaving the amyloid precursor protein by β- and γ-secretase, there are two forms of Aβ, namely Aβ40 and Aβ42. It has been found both in vitro[5,6] and in vivo[7,8] that Aβ42 aggregates faster[9] and is more toxic than Aβ40.

In vivo studies showed that senile plaques were enriched by Zn^{2+}, Fe^{3+}, and Cu^{2+}. In the case of a postmortem AD brain,[10,11] the concentration is 0.4 mM of Cu^{2+}, 1 mM of Fe^{3+}, and 1 mM of Zn^{2+}. In particular, the Zn^{2+} and Cu^{2+} is crucial, because it affects the structure and behavior of peptide aggregation. In this respect, the details of the coordination chemistry between Zn^{2+}/Cu^{2+} and Aβ have been extensively studied over the last two decades using a number of spectroscopic techniques, such as electron paramagnetic resonance, nuclear magnetic resonance (NMR), solid state NMR, circular dichroism, X-ray absorption spectroscopy, electrospray-ionization mass spectroscopy, and Raman spectroscopy, and computer simulations.[12-17] In general, a high affinity between metals and a peptide was found in the N-terminal region of 1-16 amino acids ($Aβ_{1-16}$). At physiological pH, the most acceptable binding mode for Zn^{2+} is 3N2O, which involves three nitrogen atoms (3 N) from His6, His13, and His14 residues, and two oxygen atoms (2O) from Glu11 residue.[12,14] The most commonly accepted coordination mode for Cu^{2+} is the 3N1O, which includes three nitrogen atoms from Asp1, His6, and His13 residues, and one oxygen atom from Asp1 residue.[12,17,18] These coordination modes have been used in our current work as a metal binding template, while the exact coordination modes are still under debate.[17]

Recently, X-ray crystallography[12] was unable to determine the structure of metal-Aβ complex, while several spectroscopic studies can provide only limited information.[18-31] Hence, in silico experiments were used to study the metal bound peptide in solution and were able to describe the interactions between metal ions and monomeric/oligomeric parts of Aβ in solution at the electronic, atomic, and molecular levels.[12,16,32-35] However, conflicting results have been reported. Some studies have suggested that the helical formation decrease in Aβ42[36,37] upon Zn^{2+} binding, while an opposite effect have been noticed in other studies.[38] Moreover, Huy et al[39] have recently found a lower beta sheet and helix content but a higher random coil in Aβ42–Cu^{2+}. In contrast, Liao et al[40] noted the opposite trend, that is, Cu^{2+} binding could lead to a higher beta-sheet and helix content in Aβ42, and a lower random coil content. Few investigations have estimated the solvation free energy for free and Zn^{2+} bound Aβ42 using implicit solvent model.[12] Shi et al[36] and Coskuner et al[41] have shown that the solvation free energy of Aβ42 increases upon Zn^{2+} binding, which indicates that Zn^{2+} can enhance the hydrophobicity of Aβ42. In the case of Cu^{2+} binding, the solvation free energy decreases,[39] which implies a reduced hydrophobicity of Aβ42. The opposite trend was observed by Coskuner,[41] who found that the solvation free energy increases under the influence of the same metal binding, which leads to an increase in hydrophobicity in Aβ42. In summary, contradictory results have been reported in the literature on the thermodynamic properties of Aβ peptide in the presence of metal ions, although the solvation free energy is a key thermodynamic parameter that determines the peptide hydrophobicity propensity by expressing the overall affinity of the peptide to water.[42]

To determine the hydrophobicity of Aβ42 peptide upon metal binding and determine whether the metal-peptide complexes are prone to aggregation or remain soluble in aqueous environments, we have calculated the solvation free energy, which also expresses the hydrophobicity of the peptides. To the best of our knowledge, the residual contribution of Aβ42 peptide upon metal coordination to the solvation free energy has not been discussed in the literature, and the differences in the hydrophobic propensity between the Aβ42–Cu^{2+} and Aβ42–Zn^{2+} structures have been poorly understood. In fact, the Zn^{2+} and Cu^{2+} binding with Aβ42 peptide can induce conformational changes, which may manifest in the conformational free energy landscape and the solvation free energy of Aβ42. This kind of information cannot be obtained by experimental techniques, because the disordered character of the Aβ42 in water leads to rapid conformational changes. To this end, computer simulation is particularly suitable to complement experiments. Here, we compute the residual solvation free energy of Aβ42, Aβ42–Cu^{2+} and Aβ42–Zn^{2+} and make comparison by using the three-dimensional reference interaction site model (3D-RISM) theory. In addition, we examine the structural and thermodynamic characteristics of Zn^{2+} and Cu^{2+} bound Aβ42 by using extensive (7200 ns) molecular dynamics (MD) simulation combined with the 3D-RISM theory in order to elucidate the origin of the difference in the solvation free energy between Aβ42–Cu^{2+} and Aβ42–Zn^{2+} structures. Our computer simulations unveil the reasons that Aβ42–Zn^{2+} demonstrates a stronger aggregation propensity than Aβ42–Cu^{2+} in an aqueous environment.

2 | MATERIALS AND METHODS

2.1 | Construction of the initial structure

Atomic-level details of free and metal bound Aβ peptides in aqueous media are poorly understood. Furthermore, the experimental details of coordination chemistry between transition metal ions and Aβ are still under debate. Thus far, there is no experimental structure of the

full length Aβ42–Cu^{2+} and Aβ42–Zn^{2+} peptides in the protein data bank. Hence, we carefully prepared the initial peptide structure in accordance to the following procedure: Aβ42–Cu^{2+} was constructed by combining the $A\beta_{1\text{-}16}$-Cu^{2+} model proposed by Ali-Torres et al[43] and the structure of $A\beta_{17\text{-}42}$ fragment extracted from the NMR structure (PDB id: 1IYT).[44] In this way, we obtained a full length Aβ42–Cu^{2+} model peptide, where Cu^{2+} is coordinated with the nitrogen and oxygen atoms of Asp1, N_δ of His6, and N_δ of His13.[45,46] Their binding distances are around 2.0 Å, which is very similar to previous experimental and theoretical results[12,43,47,48] (Table 1). This coordination mode was close to the physiological pH 6.9 and it was confirmed as the most stable conformation based on QM/MM studies.[43] Liao et al[40] have reported force-field parameters between Cu^{2+} and the coordination atoms used in our present simulation of Aβ42–Cu^{2+}.

The Aβ42–Zn^{2+} initial structure was constructed by combining the structure of $A\beta_{1\text{-}16}$–Zn^{2+} (PDB. id: 1ZE9)[49] with C-terminal region of $A\beta_{17\text{-}42}$ (1IYT)[44] extracted from full length Aβ42. In the metal coordination mode of this model, N_δ (His6), $O_{\varepsilon 1}$ and $O_{\varepsilon 2}$ (Glu11), N_ε (His13), and N_δ (His14) atoms are tetrahedrally coordinated with Zn^{2+} (Table 1).[36] The van der Waals radius σ = 1.10 Å and the Lennard-Jones potential well ε = 0.0125 Kcal/mol were fixed for Zn^{2+},[50] as well as for Cu^{2+}, σ = 1.20 Å and ε = 0.005 Kcal/mol.[51] Since the peptide models are generated by connecting different conformations, they are not compatible at this stage. This issue was overcome with the help of the heating-annealing simulation procedure, which we will discuss in the following section.

2.2 | MD simulation

Three different approaches have been employed to simulate metal-protein complexes: the bonded, the non-bonded, and the cationic dummy atomic models. Previous attempts with short MD simulations based on the non-bonded approach of metal interacting with peptide has been performed with limited conformational sampling.[32,33] Recently, Coskuner et al[12,41] have found that some structural features are missing at the C-terminal region of the peptides[32,33] and, in addition, various thermodynamic properties are also not provided. Hence, the role of metal ion binding in the monomeric Aβ42 structure and dynamics is still inconclusive. We have addressed this issue by performing extensive MD simulations and thermodynamic property calculations based on the bonded approach by using the AMBER16 package.[52] The Aβ42 and Aβ42–Cu^{2+} (Aβ42–Zn^{2+}) were solvated in an explicit 7100 and 7100 (9100) TIP3P[53] water separately in a cubic box and neutralized by adding Na + ions. Lindorff-Larsen et al[54] have introduced a new force field (ff99SB-ILDN), which has been used in microsecond-timescale MD simulations with explicit solvent to validate their force field against a large set of experimental NMR data that directly probe the side-chain conformations. This force field exhibits significantly better agreement with the NMR data. In addition, Man et al[55] investigated the effects of 17 widely used atomistic molecular-mechanics force-fields on the structures and kinetics of amyloid peptide assembly using 0.34 microsecond MD simulations in explicit water on the dimer of the $A\beta_{16\text{-}22}$. They have strongly recommended five force fields, namely AMBER99SB-ILDN, AMBER14SB, CHARMM22*, CHARMM36, and CHARMM36m, which are the best candidates for studying amyloid peptide assembly. Somavarapu et al demonstrated that the Aβ peptide ensembles of ff99SBildn force field are in agreement with NMR and circular dichroism data among 21 methods.[56] Therefore, we have adopted the ff99SBildn force field in the present study. The energy of each system was initially minimized by using 500 steps of the steepest descent minimization method, which were subsequently followed by 500 steps of the conjugate gradient method with the peptide being constrained by using a 500 kcal/mol-$Å^2$ harmonic potential. The system was further minimized by using 1000 steps of the steepest descent followed by 1500 steps of the conjugate gradient minimization method without restraints. After the energy minimization, the system was equilibrated as follows: Firstly, a simulation in the NVT (constant volume) ensemble for 20 ps using the Berendsen's thermostat to gradually raise the temperature from 0 to 300 K was employed. Secondly, a 200 ps NPT (constant pressure) ensemble simulation was performed to achieve the correct water density at pressure of 1 atm. Given that peptides naturally denature after being synthesized in an animal brain, the system was heated to 600 K to bring the peptide in its denatured state. Then, the system was additionally simulated for 20 ns in the canonical (NVT) ensemble at this high temperature, and then gradually annealed from 600 to 300 K by using a temperature step of 50 K. At each temperature, an NVT simulation of 1 ns was carried out. Finally, a 5 ns NPT simulation for equilibration was

TABLE 1 Force constants for the Aβ42-Cu^{2+} and Aβ42-Zn^{2+} metal complexes

Aβ42–Cu^{2+}			Aβ42–Zn^{2+}		
Bond	**Bond length (Å)**	**Force constant (Kcal/mol·$Å^2$)**	**Bond**	**Bond length (Å)**	**Force constant (Kcal/mol·$Å^2$)**
Cu–O(Asp1)	1.973	109.400	Zn–OE1(Glu11)	2.206	42.30
Cu–N(Asp1)	2.067	98.500	Zn–OE2(Glu11)	2.206	42.30
Cu–ND1(His6)	2.023	98.300	Zn–ND1(His6)	2.047	64.03
Cu–ND1(His13)	2.011	87.100	Zn–NE2(His13)	2.030	70.96
			Zn–ND1(His14)	2.047	64.03
Lennard-Jones	$R_{min}/2$ (Å)	ε (Kcal/mol)	Lennard-Jones	$R_{min}/2$ (Å)	ε (Kcal/mol)
Cu	1.20	0.05	Zn	1.10	0.012

performed at 300 K at pressure 1 atm. The last equilibrium snapshot of the simulation was then used as the initial structure (Figure 1) for production runs. The SHAKE algorithm was used to constrain the bond lengths related to hydrogen atoms.[57] The Particle Mesh Ewald (PME) method was employed for calculating the long-range electrostatic interactions,[58] while a fixed cutoff of 10 Å was used for the electrostatic and LJ potential interactions. The Langevin thermostat was used to control the temperature. The leapfrog algorithm was used to integrate the equations of motion with a time step of 2 fs.[59] Our analysis was based on 15 independent trajectories of 500 ns for all system. Hence, a total of 7500 ns (15trajectories × 500 ns) simulation of Aβ42, Aβ42–Cu^{2+} and Aβ42–Zn^{2+} was used, and the total length was 22 500 ns (22.5 μs). These independent trajectories were sufficient to investigate the structural and thermodynamic properties of the peptides.[60]

2.3 | Analysis

We analyzed the structural and thermodynamic properties of the free and metal bound Aβ peptide. Structural analysis included the calculation of the free energy landscape for at least 300 ns for each system. Thermodynamic analysis included properties, such as the total solvation free energy and the residual solvation free energy of the peptide, which was carried out by using the top 50 cluster peptide ensembles.

2.3.1 | Structural properties

Root-mean-square deviation

We have performed 500 ns simulations for the free and the metal (Cu^{2+} and Zn^{2+}) bound peptides in explicit water environment, normal physiological conditions, and room temperature. The root-mean-square deviation (RMSD)[61] of the C_α atoms as a function of time is presented in Figure 2. The RMSD values become stable for all peptides after about 200 ns of simulation, as indicated by the red colored line (equilibration time). After this time, the RMSD of all peptides fluctuates around its equilibrium value. Our analysis was carried out for times between 200 and 500 ns.

Contact map

Two residues were in contact when the distance between the center of masses of any two residues was below 5.0 Å.

Secondary structure

The secondary structure of Aβ peptide was calculated by using the DSSP (define secondary structure of protein method) program[62] in AmberTools. The average secondary structure per residue was calculated by averaging over all native and metal-bound peptide conformations acquired between 200 and 500 ns of each trajectory (Figure 3).

Solvent accessible surface area

We calculated the solvent accessible surface area (SASA) per residue with the LCPO method[64] using the CPPTRAJ program[63] in AmberTools, where the calculation was based on the spherical surface around each residue atom, at a distance of 1.4 Å away from the atoms of the van der Waals surface.

Hydrogen bonds

Hydrogen bonds were considered when the X-Y distance in X-H···Y is smaller than 3.5 Å and the X-H···Y angle is larger than 135^0.

Salt bridges

Salt bridges were identified between positively charged amino acids Arg5, Lys16, and Lys28, and negatively charged amino acids Asp1,

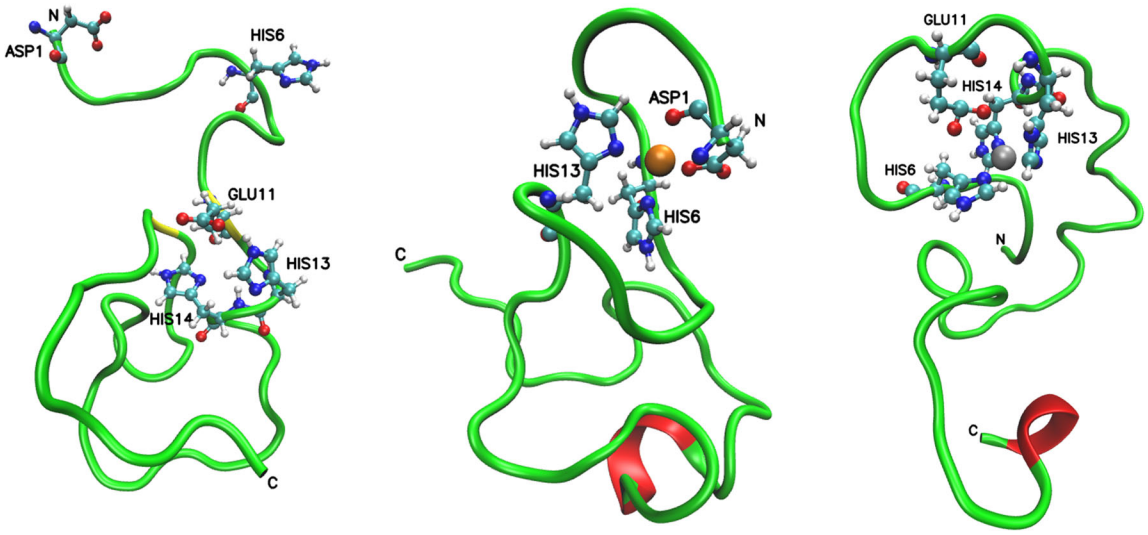

FIGURE 1 Initial structures of Aβ42(left), Aβ42–Cu^{2+} (middle), and Aβ42–Zn^{2+} (right) used in production runs are shown in "new cartoon" visual representation. Asp1, His6, Glu11, His13, and His14 residues are illustrated in Corey-Pauling-Koltun (CPK) colors, where copper and zinc are represented by orange and gray spheres, respectively, and C, N, O, and H atoms are in cyan, blue, red, and white, respectively. The color code for the peptide related to its secondary structure: red for helix, yellow for β-sheet and green for coil

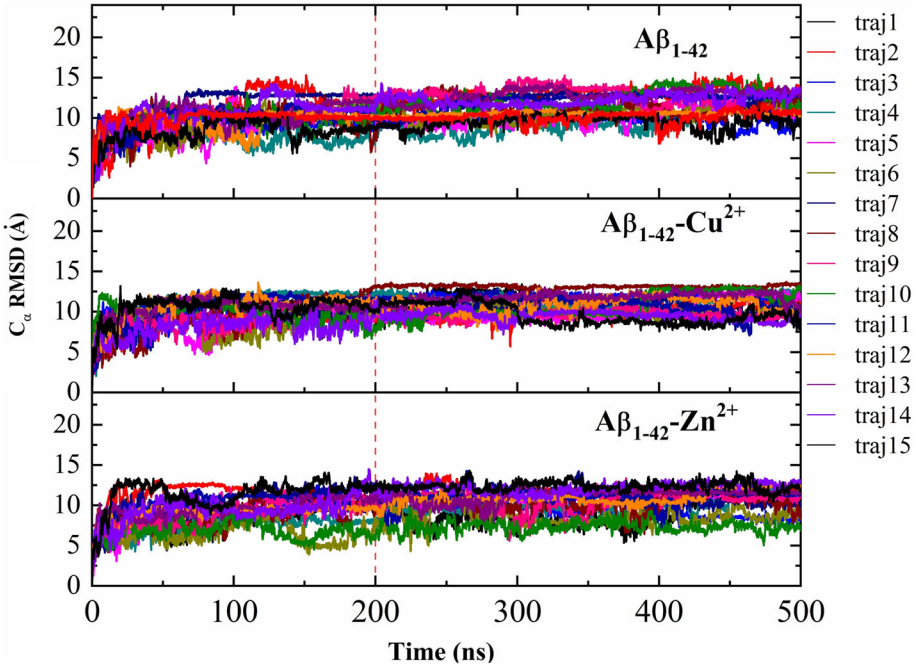

FIGURE 2 The Cα RMSD plotted against time. Red dotted line indicates to the equilibrated time 200 ns when RMSD saturates. All analyses were carried out at 200-500 ns

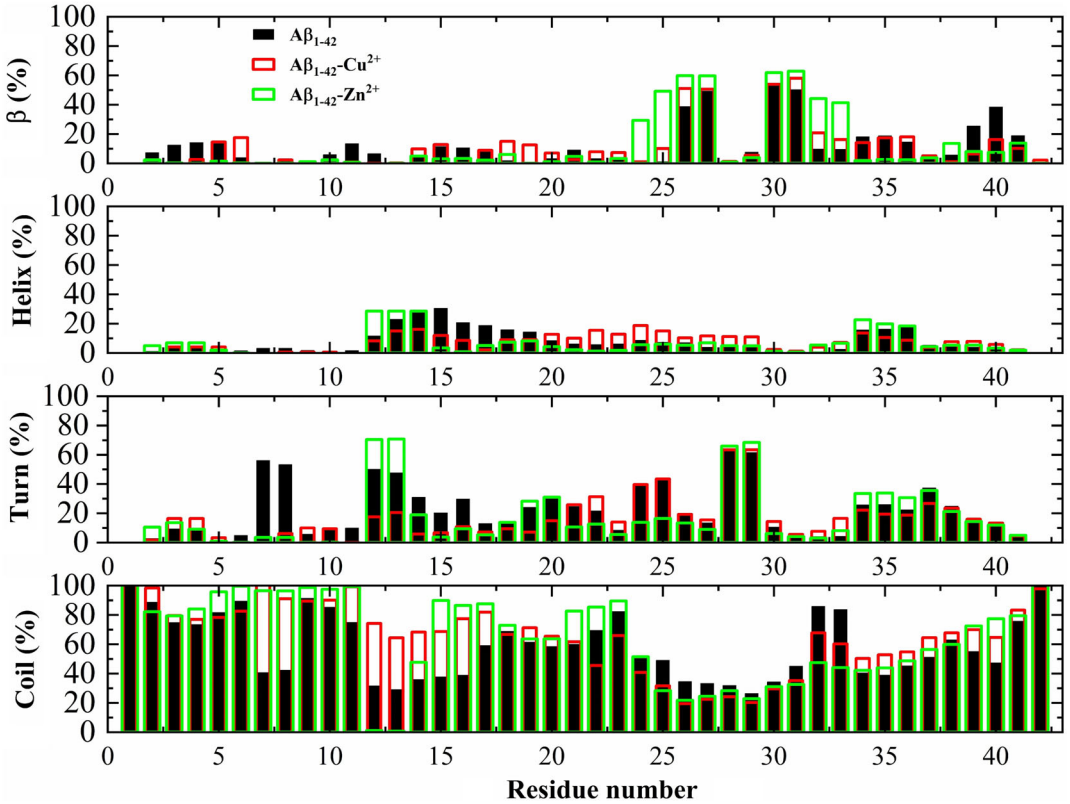

FIGURE 3 Per residue distribution of secondary structure of Aβ42, Aβ42–Cu^{2+}, and Aβ42–Zn^{2+}

Glu3, Asp7, Glu11, Glu22, and Asp23. We considered the salt bridge between two charged residues, when the distance between two specific atoms was below 4.5 Å.[64] Salt bridges between positively and negatively charged residues were determined by the following equation

$$SB = \sum_{i,j} S_{i,j}$$

$$S_{ij} = 1 \; if \; r_{i,j} \leq 0$$

$$S_{ij} = 0 \text{ if } r_{i,j} > 0$$

$$r_{i,j} = |r_i - r_j| - d_0 \quad (1)$$

where *i* and *j* are running over Nζ (Lys), Nη (Arg), Cγ (Asp), and Cδ (Glu). d_0 is the distance between atoms *i* and *j*. The value of d_0 was 4.5 Å.

Cluster analysis

The main structural features of the peptide can be predicted from representative structures, which are obtained by performing cluster analysis[65] with a RMSD cutoff of 3.0 Å.

2.3.2 | Thermo dynamic properties

Free energy landscape

We calculated the free energy surface (FES) of the systems by using two reaction coordinates, namely, V = (R_g, RMSD).[66] Then, the free energy can be expressed as

$$G(V) = -K_B T\ [\ln P(V) - \ln P_{max}] \quad (2)$$

where P(V) is the probability distribution obtained from MD simulation results. P_{max} is maximum of the distribution.

Solvation free energy

Several attempts have been made to calculate the solvation free energy of Aβ peptides using implicit solvent approaches. For example, Coskuner et al[12,13,41,67,68] and Huy et al[39] studied the thermodynamic properties using the molecular mechanics/Poisson-Boltzmann surface area method (MM/PBSA). Xu et al[69] and Shi et al[36] used the generalized Born/surface area (GB/SA) model, and Miller et al[70] used generalized born with molecular volume (GBMV) method to estimate the same properties of Aβ peptides. However, the implicit solvation models are quite different from the explicit solvent models. The simple continuum solvation models MM/PBSA, GB/SA, and GBMV have failed to account for nonpolar hydrophobic effects that play a crucial role in biological processes in water. Hence, we chose an alternative approach for the calculation of the solvation free energy that is the three-dimensional reference interaction site model (3D-RISM). Chong et al[71] developed an exact and general decomposition method of the solvation free energy that overcomes previous drawbacks. This method (see supporting information) is suitable for elucidating the molecular origin of the solvation free-energy change upon the conformational transitions of Aβ peptides in water.

Here, we have selected the top 50 peptide ensembles from the cluster analysis, and applied the 3D-RISM theory[72,73]. The solvation free energy was computed based on the Kirkwood charging equation.[74]

$$\Delta\mu = \sum_{\gamma} \rho_{\gamma} \int_0^1 d\lambda \int dr \frac{\partial u_{\gamma}^{uv}(r;\lambda)}{\partial\lambda} g_{\gamma}^{uv}(r;\lambda) \quad (3)$$

where ρ_γ denotes the average water density and λ is the charging parameter, which gradually turns on the protein-water interaction from no interaction (λ = 0, $u_\gamma(r;\lambda) = 0$) to the full interaction (λ = 1, $u_\gamma(r;\lambda) = u_\gamma(r)$). $(g_\gamma^{uv}(r;\lambda))$ is an equilibrium water distribution of water around the peptide structure and the charging parameter λ can be computed from the integral (eg, 3D-RISM theory) by using the $u_\gamma(r;\lambda)$.

Based on Chong et al,[42] $u_\gamma(r)$ expresses the interaction potential between the water site γ and peptide atoms, which consists of the pairwise additive LJ and electrostatic (elec) terms, namely $u_\gamma(r) = \sum_i \left[u_{\gamma i}^{LJ}(|r - r_i|) + u_{\gamma i}^{elec}(r - r_i)\right]$, where *i* is the peptide atom at position r_i. $u_\gamma(r)$ was substituted into the Kirkwood charging formula to obtain an exact partition of the solvation free energy into the LJ and electrostatic terms, which were further decomposed into the contributions of each peptide atom *i*. The contribution of each residue to the solvation free energy was derived from the following equation:

$$G_{solv} = G_{solv}^{LJ} + G_{solv}^{elec} = \sum_i G_i^{LJ} + G_i^{elec} \quad (4)$$

The result for G_{solv} obtained by integration is independent of the path. The most natural way is to turn on the LJ first and then the electrostatic interaction.

3 | RESULTS

3.1 | Structural properties

3.1.1 | Secondary structure analysis

Extensive in silico experiments have been performed to study the structural and thermodynamic characteristics of the Aβ peptide with and without interactions of metal ions (ie, Zn^{2+} and Cu^{2+}) in solution,[12,13,16,36,39,40,70,75] even though these characteristics remain elusive. For example, Raffa et al[75] have demonstrated that Cu^{2+} binding can promote an increase of coil formation and disruption of the β-sheet in the Aβ42 peptide. Recently, Huy et al[39] have found that the β-structures and the population of the Asp23–Lys28 salt-bridge decrease in the Aβ42–Cu^{2+} complex in comparison with the Aβ42 structure. However, the opposite trend has been observed by Liao et al,[40] who have found that Cu^{2+} binding can increase the propensity of β-sheet and salt-bridge formation in the case of Aβ42 peptide. Wise-Scira et al[13] suggested that helix formation increases and β-sheet formation decreases in the C-terminal region upon Zn^{2+} binding to Aβ42. This contrasts the results of Shi et al,[36] who found that the Zn^{2+} coordination to Aβ42 can reduce the helical structure and increase the turn formation. Given these contradictory results, the impact of metal ions (Cu^{2+} and Zn^{2+}) on the secondary and tertiary structural changes of Aβ42 peptide highlights possible problems in understanding phenomena related to the structural and thermodynamic properties of these peptide complexes. Secondary structures, such as helices, β-sheet, and turns, are crucial in studying the aggregation propensity of intrinsically disordered peptides, involved in AD.

The secondary structure content for the three peptides has been computed using the DSSP algorithm[62] and results are displayed in

TABLE 2 Average secondary-structure content for the residues Leu17–Ala42 (%) ± SD

System	β-sheet	α-helix	Turn	Coil
Aβ42	15.51 ± 9.61	6.63 ± 5.97	22.09 ± 7.39	55.77 ± 12.57
Aβ42–Cu^{2+}	16.15 ± 10.27	8.57 ± 5.76	20.84 ± 8.20	54.43 ± 10.16
Aβ42–Zn^{2+}	18.63 ± 11.78	6.06 ± 4.67	19.25 ± 5.73	56.06 ± 9.63

Figure 3 and summarized in Table 2. Interestingly, we find about 16.2% of helical formation for His13-Asp23 residues in the case of the Aβ42, whereas in the case of the Aβ42–Cu^{2+} and the Aβ42–Zn^{2+} complexes, the helical formation at the same residues decreased to ∼11.1% and ∼ 8.3%, respectively. This result suggests that the Zn^{2+} and Cu^{2+} binding reduce the helical content in His13-Asp23 residues of Aβ42. A higher tendency of β-sheet content is observed for Leu17-Ala42 residues in the case of Aβ42–Zn^{2+} (∼18.6%) and Aβ42–Cu^{2+} (∼16.1%), and to a lesser extent in the case of Aβ42 (∼15.5%). In contrast, opposite trends were found that is, lower turn contents in the case of Aβ42–Zn^{2+} (∼19.2%) and Aβ42–Cu^{2+} (∼20.8%), and higher turn in the case of Aβ42 (∼22.0%). Aβ42 has more β-sheet content (∼27%), which appears in the C-terminal hydrophobic region of Val39-Ile41 residues. For comparison, the β-sheet content is ∼16% in the case of the Aβ42–Cu^{2+} and ∼ 9% in the case of Aβ42–Zn^{2+}. This is a clear evidence that the C-terminus of Aβ42 is more rigid with respect to the Aβ42–Cu^{2+} and the Aβ42–Zn^{2+} systems. Aβ42 possesses ∼23% of turn population at the Lys33-Gly37 residues, which is stabilized by the formation of hydrogen bonds between the Gly33 and Gly37 residues. The turn facilitates two short β-sheet in the Phe29-Ile32 (∼30%) and Gly38-Ile41(∼22%) residues, which are parallel to each other due to hydrophobic interactions between Ile31 and Val39 residues. Two β-sheets (Phe29-Ile32 and Gly38-Ile41) are capped by a turn (Lys33-Gly37) and the generated hairpin structure (∼25%) in the Phe29-Ile41 residues. This result agrees well with recent high-resolution NMR results from Yan et al[76] and Colvin et al,[77] as well as simulation results by Lin et al.[78]

For both the $Aβ_{1-42}$–Zn^{2+} and Aβ42–Cu^{2+}, residues Val24-Gly33 adopt a β-hairpin conformation characterized by a type II β-turn that forms in Lys28-Gly29 residues and two short β-sheets at the loop (Val24–Asn27) and SHC (Ala30–Gly33) regions. The hairpin structure is stabilized by the backbone hydrogen-bond interactions between Asp27 and Ala30 as well as between Gly25 and Phe32 residues. These observations are consistent with the results of Wei and Shea,[79] which suggest that the monomeric state of $Aβ_{25-35}$ adopts the β-hairpin conformation in water. Surprisingly, we found that the β-hairpin population is greater (∼54%) in $Aβ_{1-42}$-Zn^{2+} compared to $Aβ_{1-42}$-Cu^{2+} (∼38%) in the Val24-Gly33 residues. This may support the fact that the former is more hydrophobic than the later.

We further observe that the interaction between CHC and SHC regions become weaker or disappear in the $Aβ_{1-42}$ structure upon Zn^{2+} binding with respect to $Aβ_{1-42}$-Cu^{2+} (Figure S1). The same trend was obtained for the interaction between the SHC and the C-terminal region. The number of contacts between the N-terminal region with the Loop and the SHC region is smaller in the $Aβ_{1-42}$ case upon Cu^{2+} binding, which is consistent with the result of obtained by Coskuner.[41] Furthermore, the interaction of the C-terminal and the loop region are stronger in the structure of $Aβ_{1-42}$ upon Zn^{2+} binding in comparison with the structure of $Aβ_{1-42}$-Cu^{2+}, implying that the aggregate of $Aβ_{1-42}$-Zn^{2+} is probably more amorphous than $Aβ_{1-42}$-Cu^{2+}. As can be seen below, this assumption is in the line with the results obtained for salt bridges. The interactions found between the C-terminus and the CHC region in the $Aβ_{1-42}$ structure are missing in the case of the $Aβ_{1-42}$-Cu^{2+} and the $Aβ_{1-42}$-Zn^{2+} complexes.

Upon Zn^{2+} binding, the interaction between N- and C-termini is much weaker compared to the Cu^{2+} binding. The Zn^{2+} interacts more with Glu11 than Cu^{2+}, with the latter being more confined to the N-terminus by Asp1. Zn^{2+} does not prefer Asp1 to Glu11, due to the more isotropic coordination achieved with Glu11. It may possible that the binding of Zn^{2+} to $Aβ_{1-42}$ can lead to the diversion of Glu11 by interactions with the C-terminus, in this way weakening the interactions between N- and C-termini (Figure S1). As for Zn/Cu competition, when Zn binds first, Cu does not bind easily, while in the case Cu binding first, Zn can bind.[80] This explanation fits with the confinement of Cu to N-terminus, while Zn is more promiscuous with the C-terminus.

3.1.2 | Salt-bridge formation

We carefully inspected the changes in the salt-bridge formation between charged residues and SASA in the peptide upon metal binding during the simulation. The presence of salt bridges in Aβ42 is an important component to maintain the fibril conformational structure.[77,81,82] In agreement with previous investigations, Arg5 establishes a salt bridge with Asp1, Glu3, Asp7, Glu11, and Glu22 residues[39-41,83] and we were able to identify all salt bridges in our simulation. In general, Aβ42 has three positively and six negatively charged residues. As a result, the formation of 18 salt bridges is possible. The presence or absence of each salt bridge was calculated for all trajectories. Figure 4 illustrates the salt bridge contact map for Aβ42, Aβ42–Cu^{2+}, and Aβ42–Zn^{2+}. In the case of Aβ42, 12 possible salt bridges were detected, hence four salt bridges, Glu3–Arg5, Glu3–Lys16, Glu11–Arg5, and Glu11–Lys16, were found to be most prevalent with 15%-30% of the population. These salt bridges are missing (or present with less probability) in the case of metal-bound peptides. This observation is consistent with the results obtained by Coskuner,[67] who found that the Glu3–Arg5 salt-bridge is highly stable in the Aβ42, and it can be disrupted after the Cu^{2+} coordination to the Aβ42.

For Aβ42–Zn^{2+}, there are four large populations (10%-30%) of salt bridges: Asp1–Arg5, Asp7–Arg5, Glu22–Arg5, and Glu22–Lys16. These populations are small in the other two structures. In particular,

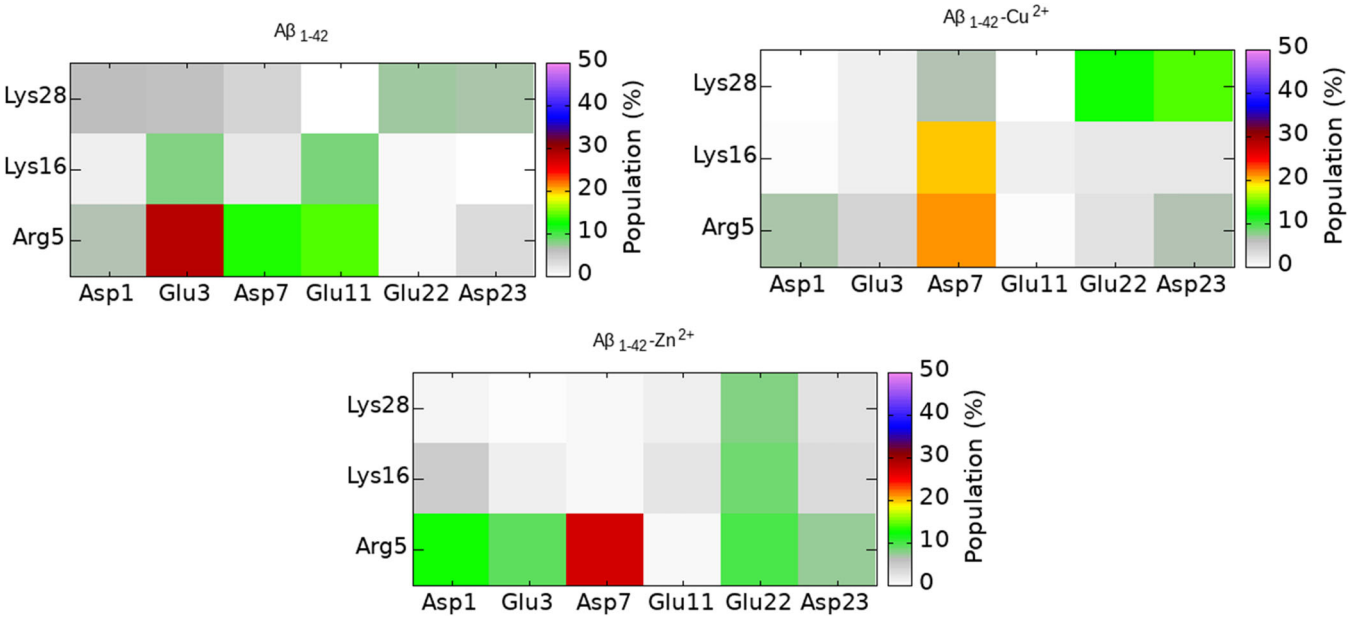

FIGURE 4 Salt-bridge contacts between charged residues in the case of the Aβ42, Aβ42–Cu^{2+}, and Aβ42–Zn^{2+} peptides

the probability of Arg5 being involved in the salt-bridge with Asp7 increases by more than 10% and 20% upon Cu^{2+} and Zn^{2+} binding to Aβ42, respectively. The same was observed by Liao et al in their study.[40] We observe that the Zn^{2+} binding causes significant structural changes in the Loop region. Glu22 forms salt bridges with Arg5 and Lys16 residues, which contributes to the cleavage of the salt bridge between Asp23 and Lys28 residues in Aβ42 upon Zn^{2+} binding. This finding agrees well with the results obtained by solid state NMR,[84] which suggest that Zn^{2+} binding can break the salt bridge between the side chains of Asp23 and Lys28 and drive these residues into nonsalt-bridge conformations, which might be the source of increased toxicity of Aβ42 at high Zn^{2+} (1:1 ratio of Aβ42:Zn^{2+}) concentrations.[85,86] In the case of Aβ42–Cu^{2+}, the Asp23-Lys28 salt-bridge is stronger compared to Aβ42 leading to stabilization of the turn conformation in the loop region. Furthermore, Cu^{2+} binding can increase the probability of Lys28 forming a salt-bridge with Glu22 and Asp23 residues in Aβ42.

Figure 5 shows the variation of the contact between Asp23 and Lys28 residues with respect to the distance between atoms Cγ of Asp23 and Nε of Lys28. A salt bridge was formed when the distance between two represented atoms is less than 5 Å. The Cu^{2+} binding to Aβ42 can induce a higher probability of the Asp23–Lys28 salt bridge formation firstly at distances between 3.5 and 4.0 Å and secondly between 5.0 and 6.0 Å. In contrast, the probability of the same salt bridge is negligible for Aβ42–Zn^{2+} at the same distances, which clearly indicates that the salt bridge occurs more frequently in the Aβ42–Cu^{2+} structure, less frequently in Aβ42, and no salt bridge forms in the case of Aβ42–Zn^{2+}. Thus, the stability of the Asp23–Lys28 salt bridge of Aβ42 drastically decreased upon Zn^{2+} binding. The higher population of Asp23–Lys28 salt bridge was noticed in the structure of Aβ42–Cu^{2+}. These findings are in good agreement

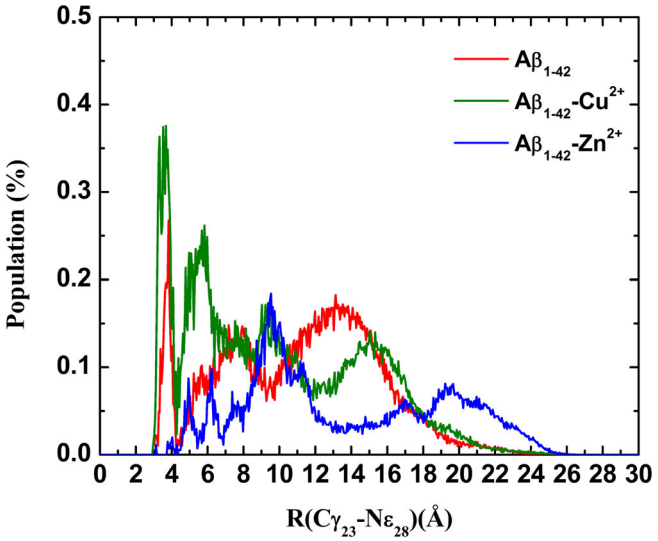

FIGURE 5 Distribution of the salt-bridge distance between atoms $C\gamma_{23}$ (Asp23) and $N\varepsilon_{28}$ (Lys28)

with the computational[40] and the solid-state NMR study,[84] which suggest that the Cu^{2+} can lead to higher stability of the salt bridge in the loop region, whereas Zn^{2+} does not. The breaking of Asp23–Lys28 might be the source of increased toxicity of Aβ42 at high Zn^{2+} (1:1 ratio of Aβ42:Zn^{2+}) concentrations.[85,86] In addition, because the Asp23-Lys28 salt bridge plays a key role in formation of cross beta fibril structure, its poor population will increase the tendency to amorphous aggregate. The Cu^{2+} binding can increase the probability of Lys28 forming a salt-bridge with Glu22 and Asp23 residues in Aβ42, suggesting that the structure of aggregate is more ordered with Cu^{2+} than Zn^{2+}.

3.1.3 | SASA analysis

In Figure S2A, Zn^{2+} coordinated residues His6, Glu11 and His13 (except His14), exhibit higher SASA values, while the same residues receive lower SASA in Aβ42–Cu^{2+}. On the other hand, Cu^{2+} coordinated residues are compelled Glu3, Gly9, Tyr10, and His14 to expose higher SASA. Interestingly, the 13 hydrophobic residues of Aβ42 (Leu17, Val18, Phe19, Phe20, Val24, Ala30, Ile31, Ile32, Leu34, Met35, Val36, Val39, and Ile41) have an increased SASA value from 11.58 ± 0.24 to 11.89 ± 0.31 and 12.18 ± 0.25 nm^2 upon Cu^{2+} and Zn^{2+} binding, respectively (Figure S2A). In other words, these hydrophobic residues showed a higher relative percentage of SASA in the case of Aβ42–Zn^{2+} than in the case of Aβ42–Cu^{2+} (Figure S2B). Hence, the intra-hydrophobic residues contact might be enhanced the SASA value in the zinc-bound peptide. Since the hydrophobicity of protein plays a key role to formation oligomers from monomer structure,[42] our result supports the fact that the Zn^{2+} binding promotes the oligomer formation propensity. This process is driven by hydrophobic collapse when hydrophobic residues become effectively shielded from water. Further details on the protein-water interaction, which can explain the hydrophobicity properties of the peptide, will be discussed in Section 3.2.2.

3.2 | Thermodynamic properties

3.2.1 | Free energy surfaces analysis

Using the cluster analysis, a total of 673, 960, and 323 clusters were obtained for Aβ42, Aβ42–Cu^{2+}, and Aβ42–Zn^{2+}, respectively (Figure 6). Among the top 200 clusters, Aβ42–Zn^{2+} has the highest cluster population in the top 40 clusters compared to Aβ42 and Aβ42–Cu^{2+}. To simplify the analysis, we used Equation (2) to calculate the FES for Aβ42, Aβ42–Cu^{2+}, and Aβ42–Zn^{2+} as a function of the radius of gyration and the C_α-RMSD (Figure 7). The FES of Aβ42 highlights four of the most populated conformations (total percentage occupied ∼15%). The local minima structures of Aβ42 are called S1-S4 and their corresponding coordinates (RMSD, Rg) are (9.7, 8.9), (9.5, 9.6), (12.0, 9.4), and (10.3, 10.0) shown in Figure 7A. In all structures, RMSD fluctuated within 9.5 to12.0 Å. The FES of Aβ42–Cu^{2+} was also characterized by four representative structures (∼17%) with the local minima structures (S1-S4) located at (8.5, 9.4), (7.2, 9.0), (6.9, 9.6), and (6.5, 9.5) (Figure 7B). In this case, the RMSD varied between 6.5 and 8.5 Å. Based on the FES calculation (Figure 7C), six representative structures (∼28%) were found for Aβ42–Zn^{2+} with the corresponding local minima structures located at (8.2, 10.1), (8.2, 9.4), (10.2, 9.7), (10.9, 9.5), (11.6, 9.11), and (9.6, 11.2), while RMSD obtained values in the range 8.2-11.6 Å. Apparently, Aβ42 is much more flexible than the metal bound Aβ42 exhibiting the largest variations in RMSD. A larger number of basins is present in the FES of Aβ42–Zn^{2+} in comparison with Aβ42–Cu^{2+} and Aβ42. This suggests that the conformational space of Aβ42–Zn^{2+} is more heterogeneous and, in agreement with the salt bridge analysis, the Aβ42–Zn^{2+} aggregate will be more amorphous compared to other cases.

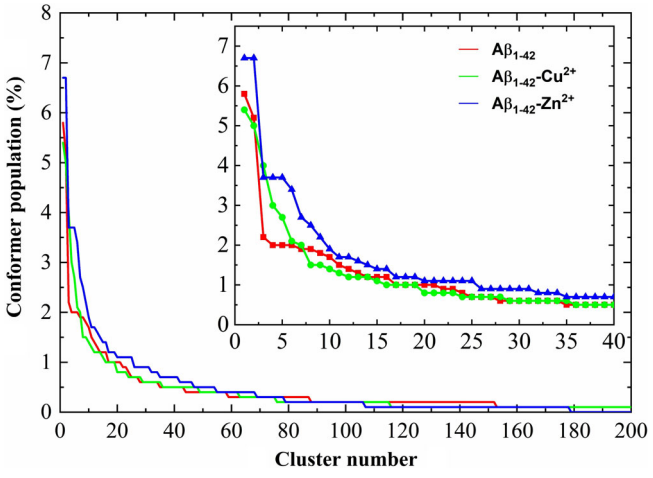

FIGURE 6 Cluster populations of Aβ42, Aβ42–Cu^{2+}, and Aβ42–Zn^{2+}. Inset shows the top 40 cluster populations of these three systems

In Aβ42, there is no helix in S3 in comparison with the other peptides (Table 3). In Aβ42–Cu^{2+}, S1, S3, and S4 are well-ordered structures having a high β-sheet content of ∼19%, ∼28%, and ∼ 19%, respectively, but S2 has a highly disordered structure due to a random coil (turn + coil), which reaches ∼93%. S1 and S3 show a boost in β-sheet content in the N-terminal region. The same trends were observed by Coskuner et al[41] in their study In the case of Aβ42–Zn^{2+}, S1, S2, and S4 have a higher β-sheet content (∼19%, ∼14%, and ∼ 19%) than in other states. A higher or lower SASA value of proteins is associated to less or more exposure to the solvent.[87] Averaging over the representative structures (Table 3) we obtained SASA are 3128 ± 169, 3242 ± 157, and 3299 ± 130 $Å^2$ for Aβ42, Aβ42–Cu^{2+}, and Aβ42–Zn^{2+}, respectively. Thus, within error bars these data show that the Zn^{2+} and Cu^{2+} binding do not change the exposure of the peptide to the water.

In Aβ42–Zn^{2+}, the two most populated conformations have the population of 6.7%, which is larger than the corresponding values of Aβ42–Cu^{2+} and Aβ42, (Table 3), where higher β-sheet and SASA values and a smaller exposure to water was observed.[87] These populated conformations are close to each other, whereas in Aβ42 and Aβ42–Cu^{2+} they are well separated. The energy barrier between the two most populated structures of Aβ42–Zn^{2+} is significantly lower than that of Aβ42–Cu^{2+} and Aβ42. Conformational exchanges mostly occur between the two most populated structures of the Aβ42–Zn^{2+} complex as each populated structure covers a larger surface area. In contrast, conformational exchanges might be difficult in the case of Aβ42 due to the high-energy barrier. These findings are in line with the results obtained from the cluster analysis where we have found that two clusters dominate in Aβ42–Zn^{2+} (Figure 6). According to the experiment, the low free energy barrier is associated with a faster aggregation propensity.[88] Thus, our results suggest that Aβ42–Zn^{2+} possess a low free energy barrier and less compactness, leading to an increased self-assembly propensity with respect to Aβ42–Cu^{2+} and Aβ42.

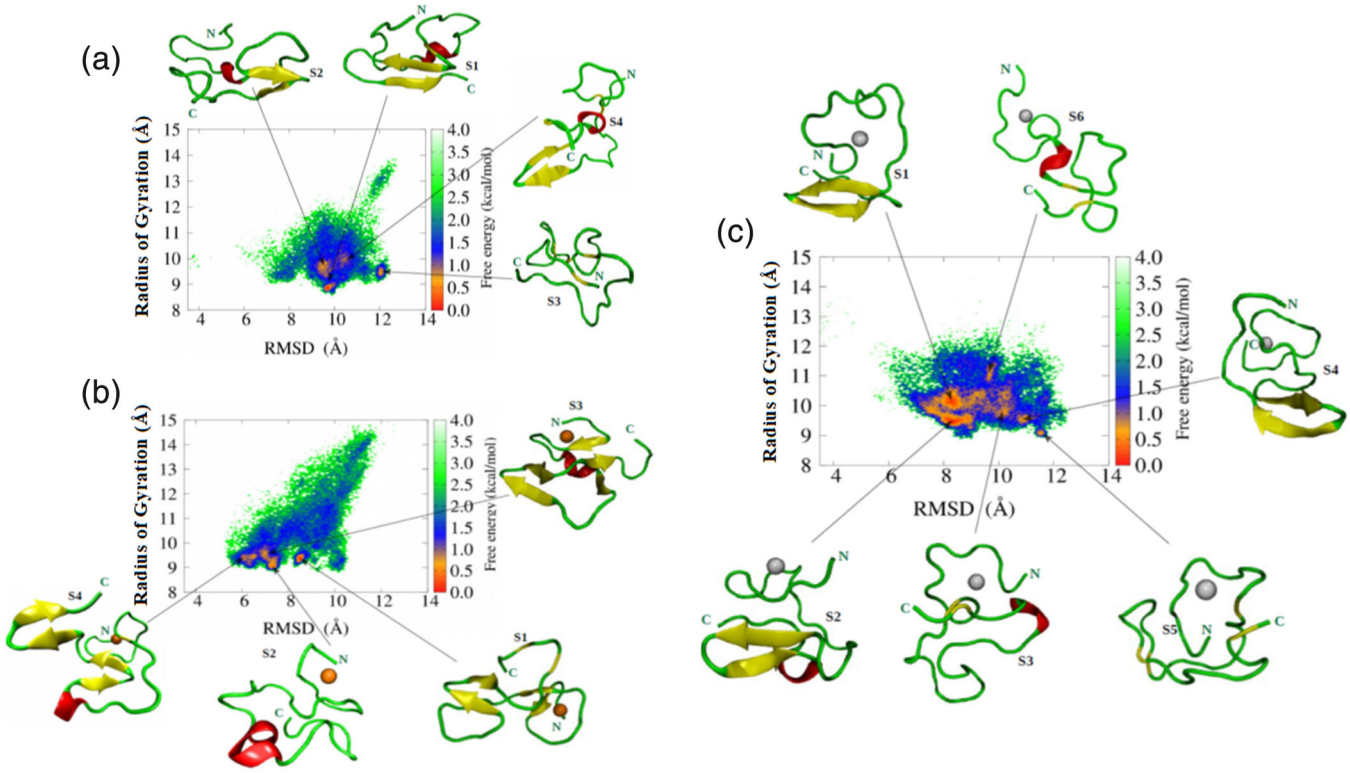

FIGURE 7 Free energy landscapes for, A, Aβ42, B, Aβ42–Cu^{2+}, and, C, Aβ42–Zn^{2+} peptides as a function of the RMSD and the gyration radius. Results are based on the whole ensemble of trajectories. Representative structures in the free-energy-minimum-basins are displayed

TABLE 3 The structural details of the most representative structures as determined by the free energy surfaces

System	State	P (%)	Rg (Å)	RMSD (Å)	HB	SASA (Å^2)	Helix (%)	β-sheet (%)	Turn (%)	Coil (%)
Aβ42	1	5.8	8.9	9.73	19	2854	16.66	16.66	16.66	50.00
	2	5.1	9.67	9.53	20	3188	7.14	9.52	9.52	73.80
	3	2.2	9.44	12.00	16	3152	0.00	9.52	21.42	69.04
	4	2.0	10.38	10.02	20	3316	7.14	19.04	26.19	47.61
Aβ42–Cu^{2+}	1	5.4	9.08	7.27	9	3108	0.00	19.04	9.52	71.42
	2	5.0	9.43	8.51	18	3067	7.14	0.00	26.19	66.66
	3	4.0	9.5	6.53	17	3431	9.52	28.57	4.76	57.14
	4	3.0	9.62	6.99	18	3361	7.14	19.04	23.80	50.00
Aβ42–Zn^{2+}	1	6.7	10.1	8.24	13	3390	0.00	19.04	16.66	64.28
	2	6.7	9.48	8.23	9	3269	7.14	14.28	16.66	61.90
	3	3.7	9.73	10.29	16	3229	7.14	4.76	26.19	61.90
	4	3.7	9.54	10.95	6	3294	0.00	19.04	9.52	71.42
	5	3.7	9.11	11.66	19	3098	0.00	9.52	19.04	71.42
	6	2.7	11.29	9.67	14	3516	14.28	4.76	16.66	64.28

We now would like to discuss the impact of the metal ions on the structural changes of peptide at the Gly29–Ala42 and the Phe24–Met35 residues, as this matter is well-connected with the aggregation mechanism. Figure 8 illustrates the structures of the most populated conformers for free and metal bound Aβ42 at Phe29–Ala42 residues. The Aβ42 conformer is well compatible with Roychaudhuri et al[89] study, who reported results of computational and experimental studies revealing a C-terminal turn at Val36–Gly37 in Aβ42, which is not present in Aβ40. Aβ42 has a more rigid Phe29–Ala42 residues than the $Aβ_{1-40}$ at the physiological temperature of 37°C. These pre-ordered residues act as internal seeds for aggregation and toxicity of Aβ42. A common feature between our simulation and the Roychaudhuri et al study[89] is that the β-hairpin conformation is formed at the Phe29–Ala42 residues of the Aβ42 peptide. In addition,

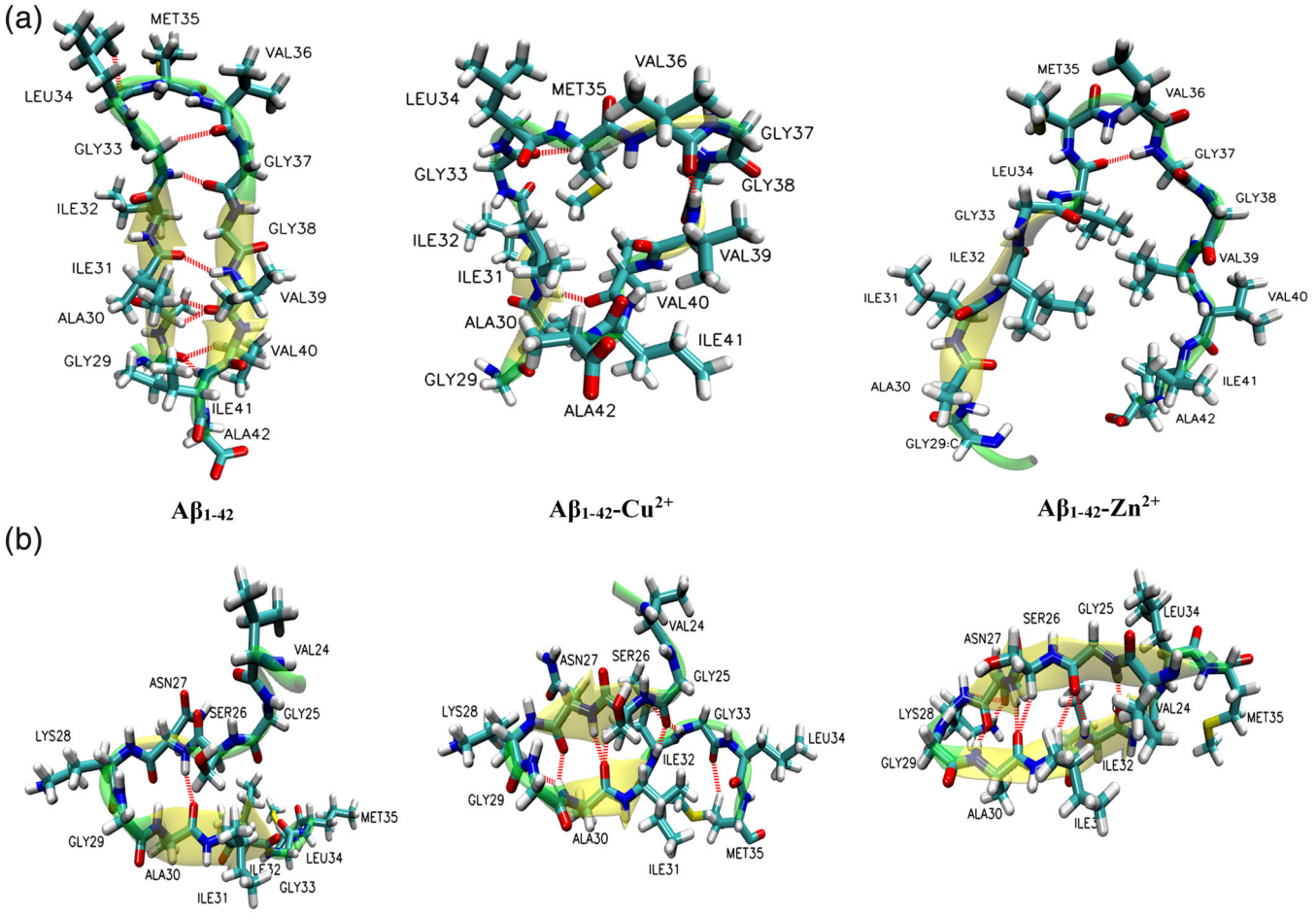

FIGURE 8 A, Structures of the most populated conformers for each peptide at the C-terminus. The turn structure is involved in residues 34-36 for Aβ42, 33-38 for Aβ42–Cu^{2+}, 34-37 for Aβ42–Zn^{2+}. Seven hydrogen bonds appear in Aβ42, three in Aβ42–Cu^{2+} and only one in Aβ42–Zn^{2+}. B, The most populated conformers for each peptide at the Val24-Met35 residues. The β-turn involves residues Lys28-Gly29 for all peptides, ribbon diagram of its own backbone to highlight the position of the backbone. Red dotted line indicates hydrogen bonds. C, N, O, H, and S atoms are in cyan, blue, red, white, and yellow, respectively

we found that hairpin conformations are stabilized by seven hydrogen bonds between β-sheets (Figure 8A). These hydrogen bonds (HBs) sharply decrease to three for Aβ42–Cu^{2+} and one for Aβ42–Zn^{2+}, which results in the absence of a β-sheet at 37-41 residues of the β-hairpin structure. In the C-terminal (Val36–Ala42) region, Aβ42 has three times higher β-sheet content in comparison with Aβ42–Cu^{2+} and 1.5 times more β-sheet content than Aβ42–Zn^{2+}. These observations indicate that the C-terminal of the Aβ42 is more rigid than Aβ42–Zn^{2+} and Aβ42–Cu^{2+}. Because the fibril formation of Aβ42 is expected to initiate from the rigid C-terminal[16] our result suggests that the aggregation of Aβ42–Zn^{2+} and Aβ42–Cu^{2+} does not necessarily begin from this end.

Figure 8B shows the most representative conformers at the Val24–Met35 for the three sequences. The Aβ42–Zn^{2+} has a higher β-hairpin population (83%) with a turn located at residues 28 and 29. We received 50% of β-hairpin population for Aβ42 and Aβ42–Cu^{2+}. This is in agreement with the results of Wei and Shea[79] who showed that most populated conformer of $A\beta_{25\text{-}35}$ is the β-hairpin. Furthermore, Aβ42 has one HB, Aβ42–Cu^{2+} seven HBs; and Aβ42–Zn^{2+} eight HBs. We find that Cu^{2+} and Zn^{2+} binding to Aβ42 introduces less mobility in residues 24-35, which may results in faster aggregation, and higher flexibility at the C-terminus (Val36–Ala42).[90-92]

3.2.2 | Solvation free energy

The protein solubility in water is an important component of the mechanism of proteins self-assembly. In particular, the protein–water interaction can be investigated by calculating the solvation free energy, which in turn can be used to identify the hydrophobicity propensity of a protein.[93-96] In particular, a larger solvation free energy is associated with increased protein hydrophobicity.[42] To this end, the hydrophobic effect is the major driving force for protein self-assembly in water. However, residual contributing hydrophobicity cannot be experimentally determined, but recent computational approaches[71,72,95,96] can estimate the hydrophobicity of a protein. In our case, the solvation free energy was computed by using the molecular theory of solvation[71-73,95,96] for the 50 most populated protein ensembles. The

average solvation free energies are summarized in Table 4. In particular, the solvation free energy of Aβ42 increases from 34.90 ± 0.98 to 59.05 ± 1.63 and 67.83 ± 1.45 kcal/mol upon Cu^{2+} and Zn^{2+} binding, respectively. In other words, the solvation free energy of Aβ42–Zn^{2+} has increased more significantly in comparison with Aβ42–Cu^{2+}. This finding suggests that the binding of Zn^{2+} rather than Cu^{2+} contributes to greater hydrophobicity of Aβ42. Furthermore, we investigated the solvation free energy for each region (Table 4), where small changes were observed in the CHC and SHC regions and significant changes in the N-terminal, loop, and C-terminal regions after Cu^{2+} and Zn^{2+} binding to Aβ42. Zn^{2+} rather than Cu^{2+} can decrease the hydrophobicity of CHC region residues Val18, Phe19, Phe20, and Ala21 and SHC region residues Gly29, Ala30, and Met35 in the Aβ42 (Table 5). Interestingly, we have overall noted that the total solvation free energies of CHC and SHC regions were decreased in case of Aβ42–Zn^{2+} (Table 4).

The solvation free energy can decrease at the Loop and the C-terminus, whereas it can increase at the N-terminal region. The average residual contributing solvation free energies are shown in Figure 9 and summarized in Table 5. In Aβ42 the contribution of Glu3, His6, Asp7, and Glu11 residues to the solvation free energy increases upon metal (Zn^{2+} and Cu^{2+}) binding, which is in good agreement with the result of Shi et al[36] and Miller et al,[70] suggesting that the Zn^{2+} coordinated residues are less exposed to water. These residues are playing a key role in enhancing the solvation free energy (hydrophobicity) in the N-terminal region of both Aβ42–Cu^{2+} and Aβ42–Zn^{2+} complexes.

We also found significant changes in the solvation free energy of positively charged residues, in particular the solvation free energy of Arg5 and Lys16 was reduced and of Lys 28 increased upon Cu^{2+} and Zn^{2+} binding. Overall, negatively (Glu3, Asp7, and Glu11) and positively (Arg5, Lys16, and Lys28) charged residues interact with water less in the case of Aβ42–Zn^{2+} than Aβ42–Cu^{2+}, which corresponds to increased solvation free energy. When His6 binds to Zn^{2+} as compared to Cu^{2+} binding, adjacent residue Asp7 is compelled to reduce the interaction with water molecules. Comparing with Aβ42–Zn^{2+}, the average solvation free energy of Asp23/Glu22 and Lys28 is greater in Aβ42–Cu^{2+} due to the higher tendency to the salt-bridge formation between Asp23 and Lys28(Figure 5), which are less exposed to water. The C-terminal residues Met35, Val36, Gly37, Gly38, Val39, and Val40 have a larger exposure to water since this region is highly disordered (high mobile) in both Aβ42–Cu^{2+} and Aβ42–Zn^{2+}. In addition, Ala42 exhibits greater solvation free energy and less exposure to water upon Zn^{2+} binding, since the contact with the N-terminus (Asp1) has a higher probability (Figure S3).

We observe three important differences for Aβ42–Zn^{2+} in comparison with Aβ42–Cu^{2+} and Aβ42. Firstly, there are three residues (Lys28, Ile31, and Ile32) that exhibit a higher hydrophobicity and lead to the stabilization of the hairpin conformation from Val24 to Met35. Secondly, the C-terminal residues Met35, Val36, Gly37, Gly38, Val39, and Val40 are highly flexible (lower solvation free energy), which allows them to actively interact with water molecules. Thirdly, seven residues Arg5, His6, Asp7, Tyr10, Glu11, His13, and His14 are actively involved in enhancing the total hydrophobicity of the N-terminal region, which leads to less exposure to water. These observations constitute a strong evidence that Zn^{2+} binding can enhance the stability of the hairpin conformation at Val24–Met35 residues while increasing the flexibility in the C-terminal region of the peptides. In other words, Aβ42–Zn^{2+} has an increased β-sheet content that occurs due to an enhanced solvation free energy, which could potentially lead to a higher hydrophobicity propensity compared to Aβ42–Cu^{2+}.

4 | DISCUSSION

The structural and thermodynamic properties of the monomeric form of the Aβ42 peptide in the presence of transition metal ions remain challenging and highly controversial to date.[12] Moreover, there have been no studies on the residual solvation free energy of Aβ42 with metal ions, despite their important role in AD. Therefore, the focus of this study is on the structural changes and the residual solvation free energy of Aβ42 in the presence of Cu^{2+} and Zn^{2+}. Our studies are based on 7200 ns of MD simulation followed by solvation free energy calculations. Much evidence has been obtained that Zn^{2+} ions promote hydrophobicity of Aβ42 peptides to a greater extent than Cu^{2+}.

We have found that Cu^{2+} and Zn^{2+} binding could lead to a higher beta-sheet and lower turn content in Aβ42. Furthermore, a higher helix and a lower random coil content were observed in Aβ42–Cu^{2+} in comparison with Aβ42 and the Aβ42–Zn^{2+} (Table 2). Regarding structural changes in metal-peptide complexes, the helical formation at His13-Asp23 residues decreases while the β-hairpin population increases at Val24-Met35 residues when Zn^{2+} and Cu^{2+} bind to Aβ42. In particular, the β-hairpin population was found to be greater in the case of Aβ42–Zn^{2+} in comparison with the structure of Aβ42–Cu^{2+} at

TABLE 4 Solvation free energy (kcal/mol) along with SD values of each region of the three peptides as determined by using the 3D-RISM theory, and *SE

Region	Aβ42	Aβ42–Cu^{2+}	Aβ42–Zn^{2+}
N-terminal (Asp1-Lys16)	−44.53 ± 47.66	19.77 ± 24.89	32.07 ± 24.61
CHC(Leu17-Ala21)	100.92 ± 7.13	99.85 ± 7.23	98.97 ± 7.66
Loop (Glu22-Lys28)	−122.98 ± 44.06	−139.54 ± 44.84	−143.40 ± 48.91
SHC(Phe29-Met35)	114.27 ± 9.58	114.03 ± 11.07	112.37 ± 10.83
C-terminal (Val36-Ala42)	−12.74 ± 22.10	−19.30 ± 29.10	−17.45 ± 32.75
Total	34.90 ± 0.98*	59.05 ± 1.63*	67.83 ± 1.45*

Note: In case of metal complex, sum of all the region is not equal to the total solvation free energy which included metal ion contribution.

TABLE 5 Residue contributions to solvation free energy ± SD. The red, blue, and black color represented in negatively, positively charged and neutral residues, respectively

Residue	Aβ42	Aβ42–Cu^{2+}	Aβ42–Zn^{2+}
ASP 1	−44.69 ± 15.82	−32.02 ± 14.35	−44.28 ± 10.24
ALA 2	10.13 ± 3.71	11.53 ± 2.21	9.82 ± 1.41
GLU 3	−78.86 ± 18.32	−57.71 ± 11.28	−51.44 ± 10.54
PHE 4	26.04 ± 3.49	23.87 ± 2.95	24.17 ± 1.98
ARG 5	71.07 ± 18.57	11.91 ± 8.76	23.21 ± 7.32
HIE 6	16.93 ± 3.92	23.50 ± 3.90	19.18 ± 2.49
ASP 7	−94.62 ± 16.25	−59.60 ± 7.38	−45.38 ± 9.81
SER 8	3.44 ± 4.62	7.88 ± 1.02	5.60 ± 1.55
GLY 9	5.77 ± 3.52	4.02 ± 2.50	3.82 ± 1.56
TYR 10	23.08 ± 4.34	19.37 ± 2.89	20.48 ± 1.43
GLU 11	−87.63 ± 14.75	2.33 ± 18.92	3.06 ± 6.31
VAL 12	20.34 ± 3.10	18.79 ± 1.75	17.65 ± 1.62
HIE 13	17.90 ± 4.56	22.34 ± 2.46	18.04 ± 1.99
HIE 14	18.11 ± 6.40	15.67 ± 2.07	17.66 ± 2.98
GLN 15	12.13 ± 6.25	10.55 ± 2.30	10.39 ± 3.63
LYS 16	36.30 ± 19.67	−2.69 ± 7.31	0.04 ± 13.51
LEU 17	22.87 ± 3.25	22.52 ± 3.28	22.58 ± 3.51
VAL 18	17.90 ± 2.74	17.20 ± 2.45	17.00 ± 2.34
PHE 19	24.80 ± 3.92	24.72 ± 3.73	24.27 ± 3.94
PHE 20	25.03 ± 3.41	24.83 ± 3.46	24.44 ± 3.56
ALA 21	10.31 ± 2.78	10.56 ± 2.26	10.66 ± 2.35
GLU 22	−99.73 ± 17.48	−117.17 ± 23.66	−121.94 ± 23.94
ASP 23	−95.24 ± 17.52	−98.40 ± 17.02	−101.81 ± 18.91
VAL 24	18.15 ± 3.20	17.55 ± 2.88	17.33 ± 3.37
GLY 25	9.11 ± 4.04	7.47 ± 3.07	7.24 ± 2.65
SER 26	7.02 ± 4.67	5.42 ± 4.27	5.26 ± 4.33
ASN 27	8.16 ± 4.95	6.05 ± 4.41	6.68 ± 3.96
LYS 28	29.54 ± 20.17	39.52 ± 29.29	43.83 ± 30.78
GLY 29	5.05 ± 2.55	4.14 ± 2.73	3.98 ± 2.64
ALA 30	11.67 ± 2.88	11.66 ± 4.14	11.21 ± 3.55
ILE 31	23.11 ± 3.16	24.44 ± 3.57	24.07 ± 3.21
ILE 32	23.24 ± 2.74	24.22 ± 3.01	24.14 ± 3.16
GLY 33	5.78 ± 3.54	6.16 ± 3.35	6.14 ± 3.41
LEU 34	23.28 ± 3.8	23.34 ± 3.61	22.77 ± 3.52
MET 35	22.10 ± 3.64	20.04 ± 3.43	20.03 ± 3.36
VAL 36	18.61 ± 2.02	16.78 ± 2.80	16.58 ± 2.95
GLY 37	4.64 ± 2.80	3.16 ± 2.57	3.50 ± 2.73
GLY 38	5.26 ± 2.94	3.82 ± 3.10	3.58 ± 3.32
VAL 39	19.27 ± 3.50	17.31 ± 3.07	17.54 ± 2.87
VAL 40	19.29 ± 3.60	18.31 ± 2.65	18.12 ± 2.25
ILE 41	22.36 ± 3.14	23.16 ± 2.87	22.78 ± 2.7
ALA 42	−102.21 ± 16.20	−101.87 ± 28.55	−99.59 ± 31.21
Cu^{2+}/Zn^{2+}	-	−15.63 ± 13.04	−14.58 ± 19.61

the Val24–Met35 residues, which is characterized by a type II β-turn formed at Lys28–Gly29 residues and two short β-sheets at the loop (Val24–Asn27) and SHC (Ala30–Gly33) regions. The hairpin is stabilized by hydrogen bonds along the backbone between Asp27 and Ala30, as well as between Gly25 and Phe32 residues. Furthermore, Cu^{2+} and Zn^{2+} can drastically decrease the β-sheet formation in the C-

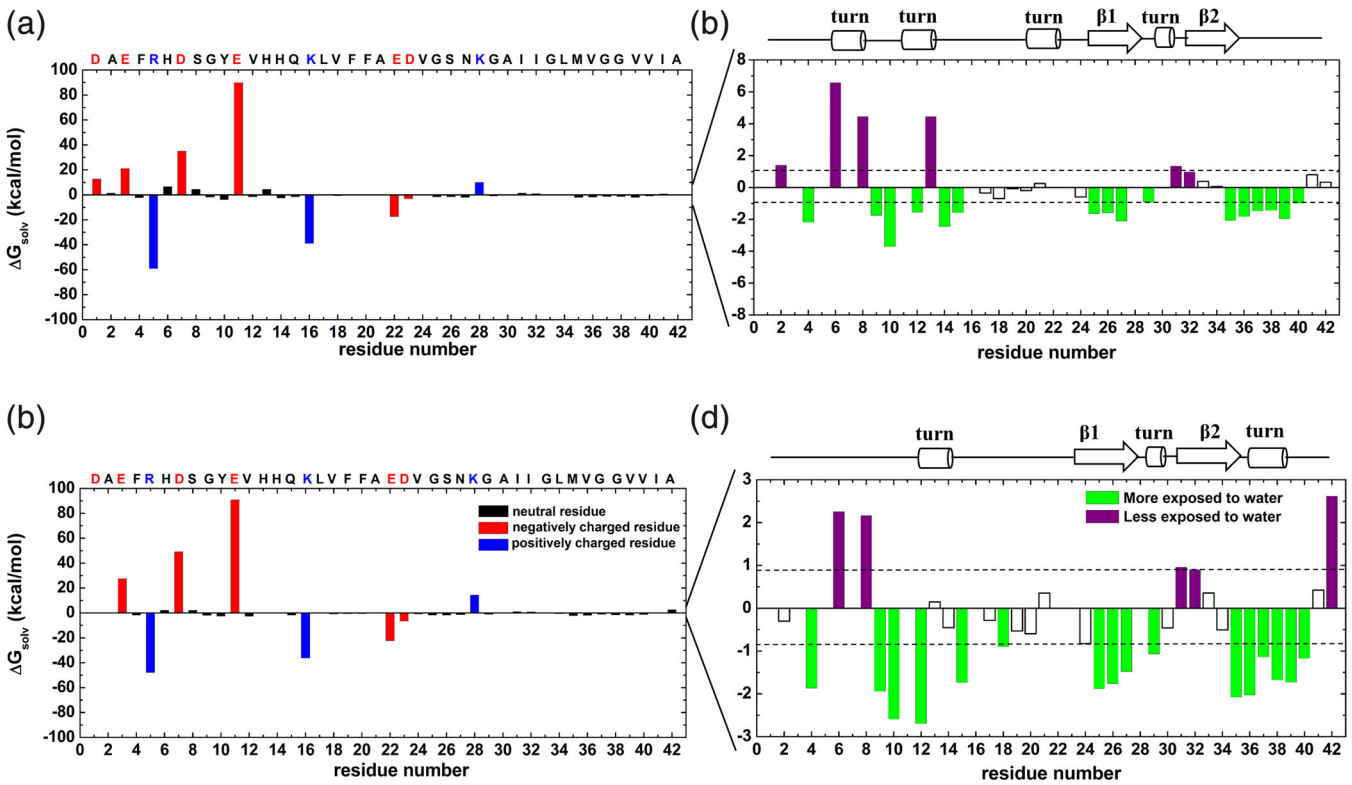

FIGURE 9 Contribution of each residue to the solvation free energy difference between Aβ42–Cu^{2+} and Aβ42, A, and, Aβ42–Zn^{2+} and Aβ42, B. Contributions from the positively charged residues are colored in blue, the negatively charged in red, and the non-charged in black. Magnified representation of the noncharged residue (C and D) contributions to ΔG_{solv}. Residues showing a ΔG_{solv} of more than 0.9 kcal/mol (in purple) were considered to be relatively less exposed to the solvent in the Cu^{2+} binding peptide than in the free peptide, whereas residues with a ΔG_{solv} of less than −0.9Kcal/mol (in green) were considered to be more exposed (positively and negatively charged residues are in blue and red, respectively). The above limits are represented as dashed lines

terminal region at Val36–Ala42 residues in Aβ42. This results in higher mobility in the C-terminal region. Finally, we studied the secondary structural properties of Aβ42. We found that, except for the metal binding region or the N-terminal region (Asp1–Lys16), the higher tendency of β-sheet contents was found for Aβ42–Zn^{2+} and Aβ42–Cu^{2+}, while a smaller value was found in the case of Aβ42. We also observe that the β-sheet formation at Leu17–Ala42 in Aβ42 is enhanced upon Zn^{2+} and Cu^{2+} binding.

The total charge of Aβ42 was reduced due to the Cu^{2+} and Zn^{2+} binding, which results in significant conformational changes with respect to free Aβ42. The most stable conformers of the peptides were found from the free energy landscape. The β-hairpin conformation is formed in Gly29–Ala42 of the Aβ42 peptide with β-sheets at Gly29–Ile32 and Gly38–Ile41 residues and a turn at Gly33–Val36 residues. This hairpin was stabilized by seven hydrogen bonds between β-sheets. These hydrogen bonds drastically decrease to three and one in the Aβ42 peptide upon Cu^{2+} and Zn^{2+} binding, respectively, which eventually destabilizes the β-hairpin structure. Hence, the C-terminal region has a higher mobility in the free peptide upon metal binding. In particular, Aβ42–Zn^{2+} acquires a relatively more ordered structure at the C-terminal region in comparison with the structure of Aβ42–Cu^{2+}.

The solvation free energy calculation can help us understand the interactions between the peptide and water. The solvation free energy of the Aβ42 peptide increases upon binding with Cu^{2+} or Zn^{2+} indicating that the metal binding can enhance the hydrophobicity of Aβ42 to promote a faster self-assembly propensity. The residual solvation free energy shows that significant changes are observed only in the N-terminal, the Loop and the C-terminal regions, where the solvation free energy can decrease in the loop and the C-terminal and increase at the N-terminus upon metal binding.

In the case of Aβ42–Cu^{2+}, the turn conformation in the loop region is stabilized by the stronger salt bridge formation between the Asp23 and Lys28 residues. In contrast to Aβ42–Zn^{2+}, the Glu22 residue involved contacts with Arg5 and Lys16 that lead to the break-up of the salt bridge (nonsalt bridge forming) and causes the destabilization of the turn structure in the loop region. The nonsalt bridge conformation may be the origin for the increased toxicity of Aβ42 with high Zn^{2+} concentration.[85,86] Overall, our findings indicate that Zn^{2+} binding during Aβ42 folding could lead to the formation of β-hairpin conformations in Val24–Met35 residues with a higher probability and a higher mobility of the C-terminal region (Val36–Val40) compared to the Cu^{2+} binding to Aβ42. This hypothesis is supported by several recent studies[70,79,84] suggesting that Val24–Met35, which adopt a hairpin structure, can induce toxicity, while Zn^{2+} binding disrupts the Asp23–Lys28 salt bridge and leads to increased hydrophobicity of oligomers.

5 | CONCLUSION

The key findings of our study are (a) Zn^{2+} binding induces a higher tendency of β-hairpin formation in Phe24–Met35 residues. This formation is stabilized by eight hydrogen bonds and the more hydrophobic nature of Ile31 and Ile32 residues, which have strong contact with Gly25 residue. However, the hairpin was destabilized in the case of Aβ42–Cu^{2+}, where a reduced number of hydrogen bonds is observed. (b) Aβ42–Zn^{2+} has a larger solvation free energy (more hydrophobic) than Aβ42–Cu^{2+}. In this case, the greater water-mediated attraction propensity has been conjectured as a factor dictating the fastest self-assembly propensity of Aβ42–Zn^{2+} than Aβ42–Cu^{2+}; c) Residual solvation free energy is suppressed in the C-terminal region (Val36, Gly37, Gly38, Val39, and Val40) upon Zn^{2+} and Cu^{2+} binding, due to the C-terminal region has a higher tendency to interact with the water molecules. This results in highly disordered structures in the case of a metal bound peptide, compared with the free peptide case.

ACKNOWLEDGMENTS

S.B. is grateful to the University of Talca, Chile, for his postdoc award through the "Fondo de Atracción de postdoctorado carácter Internacional" scheme. This research has been supported by the National Science Centre, Poland, under grant No. 2015/19/P/ST3/03541 and Department of Science and Technology, Ho Chi Minh city, Vietnam. This project has received funding from the European Union's Horizon 2020 research and innovation programme under the Marie Skłodowska-Curie grant agreement No. 665778. This research was supported in part by PLGrid Infrastructure. This work was also supported by the Polish NCN grant 2015/19/B/ST4/02721. W.G. is acknowledged to ANID-FONDECYT grant No. 1191133 and ANID-FONDEQUIP EQM160063. S.B. also acknowledges support through a one-year postdoctoral position (2016-2017) in the group of Sihyun Ham in South Korea, where the solvation free energy calculations were carried out using the PROWAVE server. We thank Giovanni la Penna for fruitful discussions and suggestions.

ORCID

Subramanian Boopathi https://orcid.org/0000-0002-9249-1112
Pham Dinh Quoc Huy https://orcid.org/0000-0002-0641-2490
Wendy Gonzalez https://orcid.org/0000-0002-7535-6883
Panagiotis E. Theodorakis https://orcid.org/0000-0002-0433-9461
Mai Suan Li https://orcid.org/0000-0001-7021-7916

REFERENCES

1. Hippius H, Neundörfer G. The discovery of Alzheimer's disease. *Dialogues Clin Neurosci*. 2003;5:101-108.
2. Prince M, Comas-Herrera A, Knapp M, Guerchet M, Karagiannidou M. World Alzheimer report 2016 improving healthcare for people living with dementia. Coverage, quality and costs now and in the future. *Alzheimer's Dis Int*. 2016;1-140.
3. Riek R, Eisenberg DS. The activities of amyloids from a structural perspective. *Nature*. 2016;539:227-235. https://doi.org/10.1038/nature20416.
4. Roychaudhuri R, Yang M, Hoshi MM, Teplow DB. Amyloid β-protein assembly and Alzheimer disease. *J Biol Chem*. 2009;284:4749-4753. https://doi.org/10.1074/jbc.R800036200.
5. Dahlgren KN, Manelli AM, Blaine Stine W, Baker LK, Krafft GA, Ladu MJ. Oligomeric and fibrillar species of amyloid-β peptides differentially affect neuronal viability. *J Biol Chem*. 2002;277:32046-32053. https://doi.org/10.1074/jbc.M201750200.
6. Maiti P, Lomakin A, Benedek GB, Bitan G. Despite its role in assembly, methionine 35 is not necessary for amyloid β-protein toxicity. *J Neurochem*. 2010;113:1252-1262. https://doi.org/10.1111/j.1471-4159.2010.06692.x.
7. McGowan E, Pickford F, Kim J, et al. Aβ42 is essential for parenchymal and vascular amyloid deposition in mice. *Neuron*. 2005;47:191-199. https://doi.org/10.1016/j.neuron.2005.06.030.
8. Iijima K, Liu H-P, Chiang A-S, Hearn SA, Konsolaki M, Zhong Y. Dissecting the pathological effects of human Aβ40 and Aβ42 in drosophila: a potential model for Alzheimer's disease. *Proc Natl Acad Sci*. 2004;101(17):6623-6628. https://doi.org/10.1073/pnas.0400895101.
9. Jarrett JT, Berger EP, Lansbury PT. The Carboxy terminus of the β amyloid protein is critical for the seeding of amyloid formation: implications for the pathogenesis of Alzheimer's disease. *Biochemistry*. 1993;32:4693-4697. https://doi.org/10.1021/bi00069a001.
10. Lovell MA, Robertson JD, Teesdale WJ, Campbell JL, Markesbery WR. Copper, iron and zinc in Alzheimer's disease senile plaques. *J Neurol Sci*. 1998;158:47-52. https://doi.org/10.1016/S0022-510X(98)00092-6.
11. Frederickson CJ, Koh JY, Bush AI. The neurobiology of zinc in health and disease. *Nat Rev Neurosci*. 2005;6:449-462. https://doi.org/10.1038/nrn1671.
12. Strodel B, Coskuner-Weber O. Transition metal ion interactions with disordered amyloid-β peptides in the pathogenesis of Alzheimer's disease: insights from computational chemistry studies. *J Chem Inf Model*. 2019;59(5):1782-1805. https://doi.org/10.1021/acs.jcim.8b00983.
13. Wise-Scira O, Xu L, Perry G, Coskuner O. Structures and free energy landscapes of aqueous zinc(II)-bound amyloid-β(1-40) and zinc(II)-bound amyloid-β(1-42) with dynamics. *J Biol Inorg Chem*. 2012;17(6):927-938. https://doi.org/10.1007/s00775-012-0909-9.
14. Xu L, Wang X, Wang X. Effects of Zn2+ binding on the structural and dynamic properties of amyloid B peptide associated with Alzheimer's disease: Asp1 or Glu11? *ACS Chem Neurosci*. 2013;4:1458-1468. https://doi.org/10.1021/cn4001445.
15. Xu L, Wang X, Shan S, Wang X. Characterization of the polymorphic states of copper(II)-bound Aβ(1-16) peptides by computational simulations. *J Comput Chem*. 2013;34(29):2524-2536. https://doi.org/10.1002/jcc.23416.
16. Nasica-Labouze J, Nguyen PH, Sterpone F, et al. Amyloid β protein and Alzheimer's disease: when computer simulations complement experimental studies. *Chem Rev*. 2015;115:3518-3563. https://doi.org/10.1021/cr500638n.
17. Atrián-Blasco E, Gonzalez P, Santoro A, Alies B, Faller P, Hureau C. Cu and Zn coordination to amyloid peptides: from fascinating chemistry to debated pathological relevance. *Coord Chem Rev*. 2018;371:38-55. https://doi.org/10.1016/j.ccr.2018.04.007.
18. Danielsson J, Pierattelli R, Banci L, Gräslund A. High-resolution NMR studies of the zinc-binding site of the Alzheimer's amyloid β-peptide. *FEBS J*. 2007;274:46-59. https://doi.org/10.1111/j.1742-4658.2006.05563.x.
19. Hou L, Zagorski MG. NMR reveals anomalous copper(II) binding to the amyloid Aβ peptide of Alzheimer's disease. *J Am Chem Soc*. 2006;128(29):9260-9261. https://doi.org/10.1021/ja046032u.
20. Talmard C, Guilloreau L, Coppel Y, Mazarguil H, Faller P. Amyloid-beta peptide forms monomeric complexes with CuII and ZnII prior to aggregation. *Chembiochem*. 2007;8(2):163-165. https://doi.org/10.1002/cbic.200600319.

21. Nair NG, Perry G, Smith MA, Reddy VP. NMR studies of zinc, copper, and iron binding to histidine, the principal metal ion complexing site of amyloid-β peptide. *J Alzheimers Dis*. 2010;20(1):57-66. https://doi.org/10.3233/JAD-2010-1346.
22. Bousejra-Elgarah F, Bijani C, Coppel Y, Faller P, Hureau C. Iron (II) binding to amyloid-β, the Alzheimer's peptide. *Inorg Chem*. 2011;50(18):9024-9030. https://doi.org/10.1021/ic201233b.
23. Syme CD, Viles JH. Solution 1H NMR investigation of Zn2+ and cd 2 + binding to amyloid-beta peptide (Aβ) of Alzheimer's disease. *Biochim Biophys Acta, Proteins Proteomics*. 2006;1764(2):246-256. https://doi.org/10.1016/j.bbapap.2005.09.012.
24. Faller P, Hureau C. Bioinorganic chemistry of copper and zinc ions coordinated to amyloid-β peptide. *Dalton Trans*. 2009;7:1080-1094. https://doi.org/10.1039/b813398k.
25. Minicozzi V, Stellato F, Comai M, et al. Identifying the minimal copper- and zinc-binding site sequence in amyloid-β peptides. *J Biol Chem*. 2008;283(16):10784-10792. https://doi.org/10.1074/jbc.M707109200.
26. Dorlet P, Gambarelli S, Faller P, Hureau C. Pulse EPR spectroscopy reveals the coordination sphere of copper(II) ions in the 1-16 amyloid-β peptide: a key role of the first two N-terminus residues. *Angew Chem Int Ed*. 2009;48(49):9273-9276. https://doi.org/10.1002/anie.200904567.
27. Hureau C, Balland V, Coppel Y, Solari PL, Fonda E, Faller P. Importance of dynamical processes in the coordination chemistry and redox conversion of copper amyloid-β complexes. *J Biol Inorg Chem*. 2009;14(7):995-1000. https://doi.org/10.1007/s00775-009-0570-0.
28. Kowalik-Jankowska T, Ruta M, Wiśniewska K, Łankiewicz L. Coordination abilities of the 1-16 and 1-28 fragments of β-amyloid peptide towards copper(II) ions: a combined potentiometric and spectroscopic study. *J Inorg Biochem*. 2003;95(4):270-282. https://doi.org/10.1016/S0162-0134(03)00128-4.
29. Shearer J, Callan PE, Tran T, Szalai VA. Cu K-edge X-ray absorption spectroscopy reveals differential copper coordination within amyloid-β oligomers compared to amyloid-β monomers. *Chem Commun*. 2010;46(48):9137-9139. https://doi.org/10.1039/c0cc02446e.
30. Viles JH. Metal ions and amyloid fiber formation in neurodegenerative diseases. Copper, zinc and iron in Alzheimer's, Parkinson's and prion diseases. *Coord Chem Rev*. 2012;256(19–20):2271-2284. https://doi.org/10.1016/j.ccr.2012.05.003.
31. Jiang D, Li X, Williams R, et al. Ternary complexes of iron, amyloid-β, and nitrilotriacetic acid: binding affinities, redox properties, and relevance to iron-induced oxidative stress in Alzheimer's disease. *Biochemistry*. 2009;48(33):7939-7947. https://doi.org/10.1021/bi900907a.
32. Boopathi S, Kolandaivel P. Role of zinc and copper metal ions in amyloid β-peptides $A\beta_{1-40}$ and $A\beta_{1-42}$ aggregation. *RSC Adv*. 2014;4(73):38951-38965. https://doi.org/10.1039/C4RA05390G.
33. Boopathi S, Kolandaivel P. Fe2+ binding on amyloid β-peptide promotes aggregation. *Proteins Struct Funct Bioinforma*. 2016;84(9):1257-1274. https://doi.org/10.1002/prot.25075.
34. Boopathi S, Kolandaivel P. Study on the inter- and intra-peptide salt-bridge mechanism of Aβ23-28oligomer interaction with small molecules: QM/MM method. *Mol BioSyst*. 2015;11(7):2031-2041. https://doi.org/10.1039/c5mb00066a.
35. Boopathi S, Kolandaivel P. Effect of mutation on Aβ42-Heme complex in aggregation mechanism: Alzheimer's disease. *J Mol Graph Model*. 2017;76:224-233. https://doi.org/10.1016/j.jmgm.2017.06.016.
36. Shi H, Kang B, Lee JY. Zn2+ effect on structure and residual hydrophobicity of amyloid β-peptide monomers. *J Phys Chem B*. 2014;118(35):10355-10361. https://doi.org/10.1021/jp504779m.
37. Pan L, Patterson JC. Molecular dynamics study of Zn(Aβ) and Zn(Aβ)2. *PLoS ONE*. 2013;8(9):e70681. https://doi.org/10.1371/journal.pone.0070681.
38. Wang W, Li W, Zhang J, Su Y, Wang J, Qin M. Effects of zinc binding on the conformational distribution of the amyloid-β peptide based on molecular dynamics simulations. *J Phys Chem B*. 2007;111(49):13814-13821. https://doi.org/10.1021/jp076213t.
39. Huy PDQ, Van Vuong Q, La Penna G, Faller P, Li MS. Impact of cu(II) binding on structures and dynamics of Aβ42 monomer and dimer: molecular dynamics study. *ACS Chem Neurosci*. 2016;7:1348-1363. https://doi.org/10.1021/acschemneuro.6b00109.
40. Liao Q, Owen MC, Olubiyi OO, Barz B, Strodel B. Conformational transitions of the amyloid-β peptide upon copper(II) binding and pH changes. *Isr J Chem*. 2017;57(7):771-784. https://doi.org/10.1002/ijch.201600108.
41. Coskuner O. Divalent copper ion bound amyloid-β(40) and amyloid-β(42) alloforms are less preferred than divalent zinc ion bound amyloid-β(40) and amyloid-β(42) alloforms. *J Biol Inorg Chem*. 2016;21(8):957-973. https://doi.org/10.1007/s00775-016-1392-5.
42. Chong SH, Ham S. Interaction with the surrounding water plays a key role in determining the aggregation propensity of proteins. *Angew Chem Int Ed*. 2014;53(15):3961-3964. https://doi.org/10.1002/anie.201309317.
43. Alí-Torres J, Mirats A, Maréchal JD, Rodríguez-Santiago L, Sodupe M. 3D structures and redox potentials of Cu2+−Aβ(1-16) complexes at different pH: a computational study. *J Phys Chem B*. 2014;118(18):4840-4850. https://doi.org/10.1021/jp5019718.
44. Crescenzi O, Tomaselli S, Guerrini R, et al. Solution structure of the Alzheimer amyloid β-peptide (1-42) in an apolar microenvironment: similarity with a virus fusion domain. *Eur J Biochem*. 2002;269(22):5642-5648. https://doi.org/10.1046/j.1432-1033.2002.03271.x.
45. Drew SC, Barnham KJ. The heterogeneous nature of Cu2+ interactions with Alzheimer's amyloid-β peptide. *Acc Chem Res*. 2011;44(11):1146-1155. https://doi.org/10.1021/ar200014u.
46. Drew SC, Noble CJ, Masters CL, Hanson GR, Barnham KJ. Pleomorphic copper coordination by alzheimer's disease amyloid-β peptide. *J Am Chem Soc*. 2009;131(3):1195-1207. https://doi.org/10.1021/ja808073b.
47. Wise O, Coskuner O. New force field parameters for metalloproteins I: divalent copper ion centers including three histidine residues and an oxygen-ligated amino acid residue. *J Comput Chem*. 2014;35(17):1278-1289. https://doi.org/10.1002/jcc.23622.
48. Parthasarathy S, Long F, Miller Y, et al. Molecular-level examination of Cu2+ binding structure for amyloid fibrils of 40-residue alzheimer's β by solid-state NMR spectroscopy. *J Am Chem Soc*. 2011;133(10):3390-3400. https://doi.org/10.1021/ja1072178.
49. Zirah S, Kozin SA, Mazur AK, et al. Structural changes of region 1-16 of the Alzheimer disease amyloid β-peptide upon zinc binding and in vitro aging. *J Biol Chem*. 2006;281(4):2151-2161. https://doi.org/10.1074/jbc.M504454200.
50. Lin F, Wang R. Systematic derivation of AMBER force field parameters applicable to zinc-containing systems. *J Chem Theory Comput*. 2010;6(6):1852-1870. https://doi.org/10.1021/ct900454q.
51. Comba P, Remenyi R. A new molecular mechanics force field for the oxidized form of blue copper proteins. *J Comput Chem*. 2002;23(7):697-705. https://doi.org/10.1002/jcc.10084.
52. Case DA, Betz R, Botello-Smith W, et al. *AMBER*. San Francisco: University of California; 2016;2016.
53. Jorgensen WL, Chandrasekhar J, Madura JD, Impey RW, Klein ML. Comparison of simple potential functions for simulating liquid water. *J Chem Phys*. 1983;79(2):926-935. https://doi.org/10.1063/1.445869.
54. Lindorff-Larsen K, Piana S, Palmo K, et al. Improved side-chain torsion potentials for the Amber ff99SB protein force field. *Proteins Struct Funct Bioinforma*. 2010;78(8):1950-1958. https://doi.org/10.1002/prot.22711.

55. Man VH, He X, Derreumaux P, et al. Effects of all-atom molecular mechanics force fields on amyloid peptide assembly: the Case of Aβ16–22 dimer. *J Chem Theory Comput*. 2019;15:1440-1452. https://doi.org/10.1021/acs.jctc.8b01107.
56. Somavarapu AK, Kepp KP. The dependence of amyloid-β dynamics on protein force fields and water models. *ChemPhysChem*. 2015;16:3278-3289. https://doi.org/10.1002/cphc.201500415.
57. Ryckaert JP, Ciccotti G, Berendsen HJC. Numerical integration of the cartesian equations of motion of a system with constraints: molecular dynamics of n-alkanes. *J Comput Phys*. 1977;23(3):327-341. https://doi.org/10.1016/0021-9991(77)90098-5.
58. Darden T, York D, Pedersen L. Particle mesh Ewald: an N·log (N) method for Ewald sums in large systems. *J Chem Phys*. 1993;98 (12):10089-10092. https://doi.org/10.1063/1.464397.
59. Hockney RW, Goel SP, Eastwood JW. Quiet high-resolution computer models of a plasma. *J Comput Phys*. 1974;14(2):148-158. https://doi.org/10.1016/0021-9991(74)90010-2.
60. Auffinger P, Louise-May S, Westhof E. Multiple molecular dynamics simulations of the anticodon loop of tRNAAsp in aqueous solution with Counterions. *J Am Chem Soc*. 1995;117(25):6720-6726. https://doi.org/10.1021/ja00130a011.
61. Roe DR, Cheatham TE. PTRAJ and CPPTRAJ: software for processing and analysis of molecular dynamics trajectory data. *J Chem Theory Comput*. 2013;9(7):3084-3095. https://doi.org/10.1021/ct400341p.
62. Kabsch W, Sander C. Dictionary of protein secondary structure: pattern recognition of hydrogen-bonded and geometrical features. *Biopolymers*. 1983;22:2577-2637. https://doi.org/10.1002/bip.360221211.
63. Weiser J, Shenkin PS, Still WC. Approximate atomic surfaces from linear combinations of pairwise overlaps (LCPO). *J Comput Chem*. 1999;20(2):217-230.
64. Bastolla U, Porto M, Roman HE, Vendruscolo M. Prinicipal eigenvector of contact matrices and hydrophobicity profiles in proteins. *Proteins Struct Funct Genet*. 2005;58(1):22-30. https://doi.org/10.1002/prot.20240.
65. Daura X, Van Gunsteren WF, Mark AE, Gademann K, Jaun B, Seebach D. Peptide folding: when simulation meets experiment. *Angew Chem Int Ed*. 1999;38(1–2):236-240. doi: 1433-7851/99/3801-0239.
66. Nguyen PH, Li MS, Stock G, Straub JE, Thirumalai D. Monomer adds to preformed structured oligomers of Aβ-peptides by a two-stage dock-lock mechanism. *Proc Natl Acad Sci U S A*. 2007;104(1):111-116. https://doi.org/10.1073/pnas.0607440104.
67. Coskuner O, Wise-Scira O, Perry G, Kitahara T. The structures of the E22Δ mutant-type amyloid-β alloforms and the impact of E22Δ mutation on the structures of the wild-type amyloid-β alloforms. *ACS Chem Neurosci*. 2013;4(2):310-320. https://doi.org/10.1021/cn300149j.
68. Wise-Scira O, Xu L, Kitahara T, Perry G, Coskuner O. Amyloid-β peptide structure in aqueous solution varies with fragment size. *J Chem Phys*. 2011;135(20):205101–205113. https://doi.org/10.1063/1.3662490.
69. Xu L, Gao K, Bao C, Wang X. Combining conformational sampling and selection to identify the binding mode of zinc-bound amyloid peptides with bifunctional molecules. *J Comput Aided Mol Des*. 2012;26 (8):963-976. https://doi.org/10.1007/s10822-012-9588-4.
70. Miller Y, Ma B, Nussinov R. Zinc ions promote Alzheimer a aggregation via population shift of polymorphic states. *Proc Natl Acad Sci*. 2010;107(21):9490-9495. https://doi.org/10.1073/pnas.0913114107.
71. Chong SH, Ham S. Atomic decomposition of the protein solvation free energy and its application to amyloid-beta protein in water. *J Chem Phys*. 2011;135(3):034506. https://doi.org/10.1063/1.3610550.
72. Chong SH, Ham S. Configurational entropy of protein: a combined approach based on molecular simulation and integral-equation theory of liquids. *Chem Phys Lett*. 2011;504(4–6):225-229. https://doi.org/10.1016/j.cplett.2011.02.006.
73. Imai T, Harano Y, Kinoshita M, Kovalenko A, Hirata F. A theoretical analysis on hydration thermodynamics of proteins. *J Chem Phys*. 2006;125(2):024911. https://doi.org/10.1063/1.2213980.
74. Ben-Naim. Molecular theory of solutions. *Mol Theory Solut* (Oxford Univ Press New York, 2006).
75. Raffa DF, Rauk A. Molecular dynamics study of the beta amyloid peptide of Alzheimer's disease and its divalent copper complexes. *J Phys Chem B*. 2007;111(14):3789-3799. https://doi.org/10.1021/jp0689621.
76. Yan Y, Wang C. Aβ42 is more rigid than Aβ40 at the C terminus: implications for Aβ aggregation and toxicity. *J Mol Biol*. 2006;364(5):853-862. https://doi.org/10.1016/j.jmb.2006.09.046.
77. Colvin MT, Silvers R, Ni QZ, et al. Atomic resolution structure of monomorphic Aβ42 amyloid fibrils. *J Am Chem Soc*. 2016;138(30):9663-9674. https://doi.org/10.1021/jacs.6b05129.
78. Lin Y, Im H, Diem LT, Ham S. Characterizing the structural and thermodynamic properties of Aβ42 and Aβ40. *Biochem Biophys Res Commun*. 2019;510(3):442-448. https://doi.org/10.1016/j.bbrc.2019.01.124.
79. Wei G, Shea JE. Effects of solvent on the structure of the Alzheimer amyloid-β(25-35) peptide. *Biophys J*. 2006;91(5):1638-1647. https://doi.org/10.1529/biophysj.105.079186.
80. De Santis E, Minicozzi V, Proux O, et al. Cu(II)-Zn(II) cross-modulation in amyloid-Beta peptide binding: an X-ray absorption spectroscopy study. *J Phys Chem B*. 2015;119(52):15813-15820. https://doi.org/10.1021/acs.jpcb.5b10264.
81. Petkova AT, Ishii Y, Balbach JJ, et al. A structural model for Alzheimer beta amyloid fibrils based on experimental constraints from solid state NMR. *Proc Natl Acad Sci*. 2002;99:16742-16747.
82. Petkova AT, Yau W, Tycko R. Experimental constraints on quaternary structure in Alzheimer's -amyloid. *Biochemistry*. 2006;45:498-512. https://doi.org/10.1021/bi051952q.
83. Linh NH, Minh Thu TT, Tu L, Hu CK, Li MS. Impact of mutations at C-terminus on structures and dynamics of Aβ40 and Aβ42: a molecular simulation study. *J Phys Chem B*. 2017;121(17):4341-4354. https://doi.org/10.1021/acs.jpcb.6b12888.
84. Mithu VS, Sarkar B, Bhowmik D, Chandrakesan M, Maiti S, Madhu PK. Zn ++ binding disrupts the asp 23-Lys 28 salt bridge without altering the hairpin-shaped cross-β structure of Aβ 42 amyloid aggregates. *Biophys J*. 2011;101(11):2825-2832. https://doi.org/10.1016/j.bpj.2011.10.023.
85. Lovell MA, Xie C, Markesbery WR. Protection against amyloid beta peptide toxicity by zinc. *Brain Res*. 1999;823(1–2):88-95. https://doi.org/10.1016/S0006-8993(99)01114-2.
86. Bishop GM, Robinson SR. The amyloid paradox: amyloid-β-metal complexes can be neurotoxic and neuroprotective. *Brain Pathol*. 2006;14(4):448-452. https://doi.org/10.1111/j.1750-3639.2004.tb00089.x.
87. David KS, Oliveira ERA, Horta BAC, Valente AP, De Paula VS. Insights into CC chemokine ligand 2/chemokine receptor 2 molecular recognition: a step forward toward Antichemotactic agents. *Biochemistry*. 2017;56(25):3197-3210. https://doi.org/10.1021/acs.biochem.7b00129.
88. Yang WY, Gruebele M. Folding at the speed limit. *Nature*. 2003;423 (6936):193-197. https://doi.org/10.1038/nature01609.
89. Roychaudhuri R, Yang M, Deshpande A, et al. C-terminal turn stability determines assembly differences between Aβ40 and Aβ42. *J Mol Biol*. 2013;425(2):292-308. https://doi.org/10.1016/j.jmb.2012.11.006.
90. Rezaei-Ghaleh N, Giller K, Becker S, Zweckstetter M. Effect of zinc binding on β-amyloid structure and dynamics: implications for Aβ

aggregation. *Biophys J*. 2011;101(5):1202-1211. https://doi.org/10.1016/j.bpj.2011.06.062.
91. Jiang D, Rauda I, Han S, Chen S, Zhou F. Aggregation pathways of the amyloid β(1 42) peptide depend on its colloidal stability and ordered β-sheet stacking. *Langmuir*. 2012;28(35):12711-12721. https://doi.org/10.1021/la3021436.
92. Miura T, Suzuki K, Kohata N, Takeuchi H. Metal binding modes of Alzheimer's amyloid β-peptide in insoluble aggregates and soluble complexes. *Biochemistry*. 2000;39(23):7024-7031. https://doi.org/10.1021/bi0002479.
93. Krupa P, Pham DQH, Li MS. Properties of monomeric Aβ42 probed by different sampling methods and force fields: role of energy components properties of monomeric Aβ42 probed by different sampling methods and force fields: role of energy components. *J Chem Phys*. 2019;151:055101. https://doi.org/10.1063/1.5093184.
94. Ben-Naim A. *Hydrophobic Interactions*. Vol 311. New York London: Plenum Press; 1980.
95. Chong S-H, Ham S. Impact of chemical heterogeneity on protein self-assembly in water. *Proc Natl Acad Sci*. 2012;109(20):7636-7641. https://doi.org/10.1073/pnas.1120646109.
96. Chong SH, Ham S. Distinct role of hydration ater in protein misfolding and aggregation revealed by fluctuating thermodynamics analysis. *Acc Chem Res*. 2015;48(4):956-965. https://doi.org/10.1021/acs.accounts.5b00032.

SUPPORTING INFORMATION

Additional supporting information may be found online in the Supporting Information section at the end of this article.

How to cite this article: Boopathi S, Dinh Quoc Huy P, Gonzalez W, Theodorakis PE, Li MS. Zinc binding promotes greater hydrophobicity in Alzheimer's Aβ42 peptide than copper binding: Molecular dynamics and solvation thermodynamics studies. *Proteins*. 2020;1–18. https://doi.org/10.1002/prot.25901